

# SOIL TEXTURE PREDICTION WITH BAYESIAN GENERALIZED ADDITIVE MODELS FOR SPATIAL COMPOSITIONAL DATA

BY JOAQUÍN MARTÍNEZ-MINAYA <sup>\*1,a</sup> ,  
LORE ZUMETA-OLASKOAGA <sup>2,3,b</sup>  AND DAE-JIN LEE <sup>4,c</sup> 

<sup>1</sup>*Department of Applied Statistics and Operational Research and Quality, Universitat Politècnica de València, Valencia, Spain*  
, <sup>a</sup>[jmarmin@eio.upv.es](mailto:jmarmin@eio.upv.es)

<sup>2</sup>*Biogipuzkoa Health Research Institute, Donostia-San Sebastián, Spain* , <sup>b</sup>[lore.zumetaolaskoaga@bio-gipuzkoa.eus](mailto:lore.zumetaolaskoaga@bio-gipuzkoa.eus)

<sup>3</sup>*Deusto Physical Therapist, Faculty of Health Sciences, University of Deusto, Donostia-San Sebastián, Spain*

<sup>4</sup>*School of Science and Technology, IE University, Madrid, Spain* , <sup>c</sup>[daejin.lee@ie.edu](mailto:daejin.lee@ie.edu)

Compositional data (CoDa) plays an important role in many fields such as ecology, geology, or biology. The most widely used modeling approaches are based on the Dirichlet and the logistic-normal formulation under Aitchison geometry. Recent developments in the mathematical field on the simplex geometry allow to express the regression model in terms of coordinates and estimate its coefficients. Once the model is projected in the real space, we can employ a multivariate Gaussian regression to deal with it. However, most existing methods focus on linear models, and there is a lack of flexible alternatives such as additive or spatial models, especially within a Bayesian framework and with practical implementation details.

In this work, we present a geoadditive regression model for CoDa from a Bayesian perspective using the `brms` package in R. The model applies the isometric log-ratio (ilr) transformation and penalized splines to incorporate nonlinear effects. We also propose two new Bayesian goodness-of-fit measures for CoDa regression: BR-CoDa- $R^2$  and BM-CoDa- $R^2$ , extending the Bayesian  $R^2$  to the compositional setting. These measures, alongside WAIC, support model selection and evaluation. The methodology is validated through simulation studies and applied to predict soil texture composition in the Basque Country. Results demonstrate good performance, interpretable spatial patterns, and reliable quantification of explained variability in compositional outcomes.

**1. Introduction.** Understanding the spatial distribution and variability of soil texture is essential for land use planning and other activities related to agricultural management and environmental protection (e.g., prevent soil degradation, preserve soil functions and remediate degraded soil). This work is motivated by the “Land Use and Cover Area frame Statistical survey” (LUCAS) project aimed at collecting harmonized data on the state of land use/cover over the extent of the European Union. The study by [Ballabio, Panagos and Monatanarella \(2016\)](#) mapped soil properties at a continental scale across Europe. In this work, we aim to map soil texture distribution at a finer scale based on soil samples (at 30 cm depth) surveyed in the Basque Country (Spain) between 2010 and 2018.

Soil texture data are usually treated as compositional data (i.e., relative percentages of different particles: sand, silt and clay, whose sum is constrained to 100%). Consequently, analyzing each texture component separately may lead to inconsistent results, such as total values exceeding 100%. CoDA is the common acronym of Compositional Data Analysis.

---

\*[Corresponding author]

*Keywords and phrases:* Bayesian inference, CoDa, Bayesian CoDa- $R^2$ , Spatial, Generalized Additive Models, Penalized splines.

CoDA theory provides the statistical framework for compositional data, which lies in a simplex sample space (Aitchison and Lauder, 1985). In addition to soil texture samples, we incorporate auxiliary information such as climatic variables (e.g., average precipitation, minimum and maximum temperatures), topographic features (e.g., digital elevation model—DEM), and categorical variables including geological characteristics (e.g., lithology) and land use types (e.g., pastures, extensive crops, vineyards).

Moreover, CoDA is widely applied in other fields such as the analysis of chemical and mineralogical compositions (Zhou et al., 2018), economics (Wang, Wang and Wang, 2019), environmental studies of air pollution (AL-Dhurafi, Masseran and Zamzuri, 2018; Mota-Bertran, Saez and Coenders, 2022), research on physical activity and health, and microbiome studies (Combettes and Müller, 2020; Creus Martí, Moya and Santonja, 2022). Indeed, while the mathematical and statistical foundations of CoDA have been widely developed (Pawlowsky-Glahn and Buccianti, 2011; Pawlowsky-Glahn, Egozcue and Tolosana-Delgado, 2015; Pawlowsky-Glahn and Egozcue, 2016), contributions from the statistical modelling perspective remain limited, despite their considerable potential. These include non-parametric density estimation and regression for compositional data (Chacón and Duong, 2010; Di Marzio, Panzera and Venieri, 2015), model and variable selection (Lin et al., 2014; Susin et al., 2020), model diagnostics (Hijazi, 2008), and the development of open-source software tools to support applied researchers working with CoDA (Comas Cufí et al., 2011; Lin et al., 2014).

Incorporating geographical information into the model is crucial when the underlying process exhibits spatial dependence. Possible approaches include extending the ordinary kriging to CoDA (wen Zhang et al., 2013), introducing a conditional autoregressive (CAR) component for discrete spatial domains (Martinez et al., 2020), using a continuous Gaussian field for continuous spaces (Martínez-Minaya and Rue, 2024; Mota-Bertran, Saez and Coenders, 2022; Pirzamanbein et al., 2018), or employing spatial models with many zeros (Leininger et al., 2013; Figueira et al., 2025). In this work, we focus on extending the CoDa regression within the generalized additive models (GAM) framework. GAMs provide a flexible approach to include nonlinear terms, or smooth interactions such as tensor products for spatial anisotropic effects or varying-coefficient terms among other structures (Wood, 2017). The availability of open source software R and packages for GAMs such as `mgcv`, facilitates the use of these powerful tools by researchers and practitioners across various fields. Moreover, Bayesian implementations of GAMs and other regression structures (such as multilevel models) are supported by the `brms` R package, developed by Bürkner (2017), which provides a high-level R front-end for a wide variety of model types, all fitted using the probabilistic programming language Stan (Betancourt and Girolami, 2015; Carpenter et al., 2017). Recently, Thomas (2020) proposed the R package `bayesGAM`, which is designed to fit univariate and multivariate response GAMs using Hamiltonian Monte Carlo (HMC).

Model evaluation in CoDA has received increasing attention in recent years. Various approaches have been proposed, including the use of Bayesian model selection criteria such as the Watanabe–Akaike Information Criterion (WAIC; Gelman, Hwang and Vehtari 2014), leave-one-out cross-validation (LOOCV), and automatic group construction procedures for leave-group-out cross-validation (LGOVCV) adapted for latent Gaussian models fitted via INLA (Adin et al., 2024; Martínez-Minaya and Rue, 2024). These methods support model comparison and out-of-sample validation in compositional frameworks. However, a limitation of these approaches is that they do not provide an interpretable summary of explained variability, analogous to the classical  $R^2$ .

To fill this gap, we propose two novel Bayesian measures of explained variance in CoDa models, BR-CoDa- $R^2$  and BM-CoDa- $R^2$ , which extend the concept introduced by Gelman et al. (2019) to the compositional domain using the `ilr` transformation. These measures respect

the geometry of the simplex and offer a principled way to assess model fit in flexible regression settings. In this regard, we also show how CoDa regression can naturally be extended to nonlinear and spatial frameworks through Bayesian GAMS.

The paper is structured as follows. In [section 2](#), we provide an overview of the soil texture survey conducted in the Basque Country. In [section 3](#), we introduce the fundamental concepts of the simplex space underlying CoDa and its associated geometry. In [section 4](#), we present the foundations of simplicial regression and generalized additive models (GAMs), and describe how these structures are defined within a Bayesian framework. In [section 5](#), we introduce several Bayesian model selection and validation criteria, which lead to the presentation of our proposed Bayesian CoDa- $R^2$  measures in [section 6](#). [section 7](#) presents a series of simulation studies that evaluate the performance of the proposed methodology and the goodness-of-fit measures introduced, followed by a real-data application in [section 8](#). Finally, [section 9](#) summarizes the main findings and outlines potential avenues for future research.

**2. Soil texture survey in the Basque Country.** Soil texture is one of the most fundamental soil characteristics. It influences various physical, chemical, biological, and hydrological properties and processes, such as water and nutrient retention and infiltration. It is commonly determined by sedimentation methods using a pipette or a hydrometer, which provides the relative proportion of soil mineral particles: sand whose particle diameter varies between 2.00 and 0.05 *mm*; silt, which varies between 0.05 and 0.002 *mm*; and clay, whose diameter is lower than 0.002 *mm*. As previously stated, soil particle-size fractions are treated as CoDa.

In recent years, numerous studies have proposed different approaches to map soil texture. Notable examples include [Adhikari et al. \(2013\)](#) and [Ballabio, Panagos and Monatanarella \(2016\)](#). Among other methods, [Akpa et al. \(2014\)](#) and [Chagas et al. \(2016\)](#) use random forest and multiple linear regression; [Niang et al. \(2014\)](#), [Gooley et al. \(2014\)](#) or [Hengl et al. \(2014\)](#), employ techniques such as kriging and Supported Vector Machine (SVM); [Wadoux and Molnar \(2021\)](#) conduct analysis with interpretable Machine Learning methods or [Swetha et al. \(2020\)](#) with convolutional neural network (CNN) algorithms; and authors such as [Buchanan et al. \(2012\)](#) who compare ordinary kriging with Geoadditive models, [Poggio and Gimona \(2017\)](#) who use hybrid geostatistical GAMs or [Nussbaum et al. \(2017\)](#) who employs boosted geoadditive models. In most cases, covariates used in the models were derived from the DEM and remote sensing.

The spatial distribution of soil texture plays a key role in many of these approaches, as it can help address major global environmental challenges such as climate change, food and water scarcity, and biodiversity loss ([Hartemink and McBratney, 2008](#)). However, the relevance of spatial effects is not limited to this context. In many CoDa problems, incorporating spatial components is crucial for improving predictive performance. Spatial CoDa problems can be defined over discrete domains, where autoregressive spatial effects are required ([Martinez et al., 2020](#)), or over continuous domains, where classical kriging methods are typically employed ([Pawłowsky-Glahn and Egozcue, 2016](#); [wen Zhang et al., 2013](#)). From a Bayesian perspective, several authors have also addressed this problem ([Pirzamanbein et al., 2018](#); [Martínez-Minaya and Rue, 2024](#)). GAMs offer a suitable approach for integrating geographic information. They enable the inclusion of effects such as elevation in a nonlinear fashion, providing greater flexibility to explain the phenomena of interest ([Hastie and Tibshirani, 1990](#)). Thus, the combination of GAMs and CoDa provides an ideal methodological framework for mapping soil texture in our study area, the Basque Country (Spain).

The available data consist of 2279 soil samples (at 30 *cm* depth) surveyed in the Basque Country between 2010-2018 ([Figure 1](#)), work carried out by the Basque Institute for Agricultural Research and Development (<https://neiker.eus/en/>). Variables such as Elevation, Slope,

and Lithology were obtained from <https://www.geo.euskadi.eus/>. The spatial resolution of the covariates was  $500\text{ m} \times 500\text{ m}$ . See Figure 1 for a graphical representation of the study area and covariates, and Table 1 for a detailed description of the Lithology factor levels.

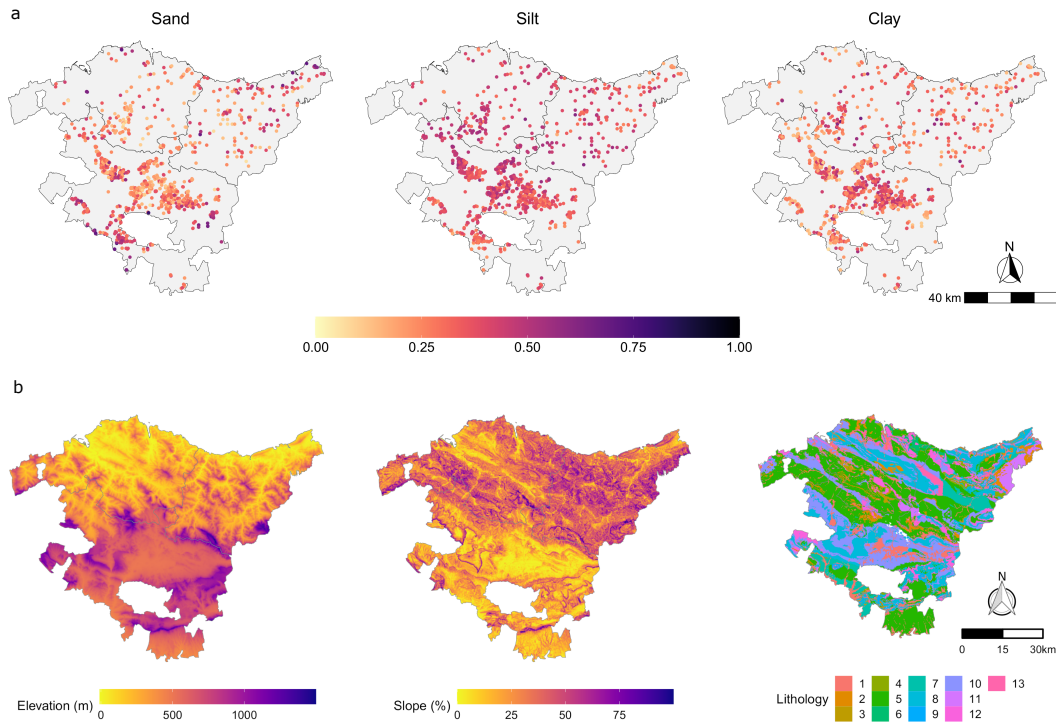


FIG 1. (a) Map of the study area showing the relative abundances of sand, silt, and clay at each sampling location. (b) Map of the study area showing the three covariates used in the analysis: elevation, slope, and lithology.

TABLE 1  
Categorical levels of the Lithology covariate used in the modeling framework.

Factor level	Description
1	Surface Deposits
2	Coarse-grained detrital rocks (sandstones). Dominant
3	Medium-grained detrital rocks (siltstones). Dominant
4	Fine-grained detrital rocks (shales). Dominant
5	Alternating detrital clasts
6	Decarbonate marls
7	Marls
8	Impure limestones and calcarenites
9	Clays with gypsum and other salts
10	Alternation of marl limestones, chalky marls and calcarenites
11	Slates
12	Limestones and dolomites
13	Volcanic rocks

**3. The simplex and its geometry.** CoDA relies on understanding the mathematical structure of the simplex, the appropriate sample space in which compositions reside. Unlike

traditional Euclidean space, the simplex imposes specific constraints, such as the constant sum of the components, which require specialized geometric tools to properly describe and analyze the data. In this section, we introduce the essential concepts of Aitchison geometry, which allow us to define operations such as distance, orthogonality, and inner products for CoDa. We then describe the isometric log-ratio (ilr) transformation, a key tool that allows mapping data from the simplex to an unconstrained Euclidean space, thereby enabling the application of classical statistical techniques. Lastly, we explore statistical summaries within the simplicial framework, including the definitions of center and variance in the context of CoDA, providing the foundation for the modeling approaches that follow.

**3.1. Aitchison Geometry.** A composition is a  $D$ -component vector whose components show the relative importance of  $D$  parts forming a total. It is characterized by the fact that only relative information is relevant, scaling it by any constant values does not change its meaning (Aitchison, 1982).

The simplex,  $\mathcal{S}^D$ , is the sample space of CoDa, and it is commonly defined as:

$$(1) \quad \mathcal{S}^D = \left\{ \mathbf{y} = [y_1, \dots, y_D]; y_d > 0, d = 1, 2, \dots, D; \sum_{d=1}^D y_d = \kappa \right\},$$

being  $\kappa$  an arbitrary positive constant, *e.g.*,  $\kappa = 1$  if measurements are performed in parts per unit (proportions) or  $\kappa = 100$  if they are in percentages. From now on, and without loss of generality, we assume that  $\kappa = 1$ . As in the ordinary real Euclidean space, a specific geometry is defined in the simplex, also known as simplicial geometry. It does not follow ordinary Euclidean rules observed in real vector space. Nevertheless, concepts such as distance between points, straight lines, orthogonality, norm, and inner vector product exist for a simplex vector space (Egozcue and Pawłowsky-Glahn, 2011).

Perturbation denoted by  $\oplus$  (an internal operation) and powering denoted by  $\odot$  (an external operation) are defined as the two main operations in the simplex. They correspond to addition and scalar multiplication in the real space. Thus, if  $\mathbf{z}, \mathbf{y} \in \mathcal{S}^D$ , perturbation in the simplex is defined as

$$(2) \quad \mathbf{z} \oplus \mathbf{y} = \frac{[z_1 y_1, \dots, z_D y_D]}{z_1 y_1 + \dots + z_D y_D} = \mathcal{C}(z_1 y_1, \dots, z_D y_D),$$

where  $\mathcal{C}$  denotes the closure operator which standardizes the vector dividing each component by the sum of its components. Similarly, for any real number  $\alpha$ , the powering operation is defined as:

$$(3) \quad \alpha \odot \mathbf{y} = \mathcal{C}(y_1^\alpha, \dots, y_D^\alpha).$$

Moreover, an inner product  $\langle \cdot, \cdot \rangle_a$  can be established

$$(4) \quad \langle \mathbf{z}, \mathbf{y} \rangle_a = \sum_{d=1}^D \log \frac{z_d}{g_m(\mathbf{z})} \log \frac{y_d}{g_m(\mathbf{y})},$$

where  $g_m(\mathbf{z})$  and  $g_m(\mathbf{y})$  denote the geometric mean of the components of  $\mathbf{z}$  and  $\mathbf{y}$  respectively. With all these operations,  $(\mathcal{S}^D, \oplus, \odot, \langle \cdot, \cdot \rangle_a)$  has a  $(D-1)$ -dimensional real Euclidean vector space structure, and the geometry defined on the simplex is named simplicial or Aitchison geometry (Pawłowsky-Glahn and Egozcue, 2001).

The related norm  $\|\cdot\|_a$  and distance  $d_a(\cdot, \cdot)$  are defined as:

$$(5) \quad \|\mathbf{y}_a\| = \langle \mathbf{y}, \mathbf{y} \rangle_a^{(1/2)},$$

and

$$(6) \quad d_a(\mathbf{z}, \mathbf{y}) = \|\mathbf{z} \ominus \mathbf{y}\|_a,$$

being  $\ominus$  the subtraction operation defined as  $\mathbf{z} \ominus \mathbf{y} = \mathbf{z} \oplus (-1) \odot \mathbf{y}$ .

3.2. *The isometric log-ratio transformation (ilr).* Due to the Euclidean structure of  $\mathcal{S}^D$ , an orthonormal basis with respect to the inner product can be constructed (Egozcue et al., 2003), and a composition  $\mathbf{y} \in \mathcal{S}^D$  can be represented by its coordinates with respect to such a basis:

$$(7) \quad \mathbf{y} = \bigoplus_{d=1}^{D-1} \mathbf{y}_d^* \odot \mathbf{e}_d, \quad \mathbf{y}_d^* = \langle \mathbf{y}, \mathbf{e}_d \rangle_a,$$

where  $\{\mathbf{e}_1, \dots, \mathbf{e}_{D-1}\}$  is an orthonormal basis of  $\mathcal{S}^D$ , and  $\mathbf{y}^* = [y_1^*, \dots, y_{D-1}^*]$  denotes the coordinate vector of  $\mathbf{y}$  with respect to the selected basis. The function  $\text{ilr}: \mathcal{S}^D \rightarrow \mathbb{R}^{D-1}$ , which assigns the coordinates  $\mathbf{y}^*$  to  $\mathbf{y}$ , i.e.  $\text{ilr}(\mathbf{y}) = \mathbf{y}^*$ , is called isometric log-ratio transformation, and constitutes an isometric isomorphism between vector spaces (Pawlowsky-Glahn, Egozcue and Tolosana-Delgado, 2015).

As  $\text{ilr}(\mathbf{y}) \in \mathbb{R}^{D-1}$  can be identified with the coordinates of  $\mathbf{y} \in \mathcal{S}^D$  with respect to the basis  $\{\mathbf{e}_1, \dots, \mathbf{e}_{D-1}\}$ , it can also be identified with coordinates with respect to the canonical basis in  $\mathbb{R}^{D-1}$ ,  $\{\mathbf{e}_1^*, \dots, \mathbf{e}_{D-1}^*\}$ . This brings us to the equivalent definition of ilr coordinates:  $\text{ilr}(\mathbf{y}) = \sum_{d=1}^{D-1} \langle \mathbf{y}, \mathbf{e}_d \rangle_a \mathbf{e}_d^*$ , where  $\text{ilr}(\mathbf{e}_d) = \mathbf{e}_d^*$ ,  $d = 1, \dots, D-1$ . As pointed out in Egozcue et al. (2003), the inverse ilr transformation corresponds to the reconstruction of  $\mathbf{y}$  in the reference basis of  $\mathcal{S}^D$ .

$$(8) \quad \mathbf{y} = \text{ilr}^{-1}(\mathbf{y}^*) = \bigoplus_{d=1}^{D-1} (\langle \mathbf{y}^*, \mathbf{e}_d^* \rangle \odot \mathbf{e}_d).$$

Among the various ways to define orthonormal bases in  $\mathcal{S}^D$ , the most popular due to its interpretability are those bases linked to a sequential binary partition (SBP) of the compositional vector (Egozcue and Pawlowsky-Glahn, 2005; Pawlowsky-Glahn and Buccianti, 2011). The main appeal of such bases is that they are easily interpreted in terms of grouped parts of the composition. The Cartesian coordinates of a composition in such a basis are called balances.

In this work, we focus on a particular SBP obtained by Egozcue et al. (2003) using the Gram-Schmidt procedure, easily computed through the R-package `compositions` (van den Boogaart, Tolosana-Delgado and Bren, 2021). In particular, the basis elements  $\mathbf{e}_d$ ,  $d = 1, \dots, D-1$ , are defined as follows,

$$(9) \quad \mathbf{e}_d = \mathcal{C} \left[ \exp \left( \underbrace{\left( \sqrt{\frac{1}{d(d+1)}}, \dots, \sqrt{\frac{1}{d(d+1)}} \right)}_{d \text{ elements}}, -\sqrt{\frac{d}{d+1}}, 0, \dots, 0 \right) \right],$$

and they are orthonormal with respect to the Aitchison inner product (Equation 4) and they are a basis of  $\mathcal{S}^D$ . The components of  $\mathbf{y}^* = \text{ilr}(\mathbf{y})$  with respect to the basis (Equation 9) are:

$$(10) \quad y_d^* = \sqrt{\frac{d}{d+1}} \log \left[ \frac{g_m(y_1, \dots, y_d)}{y_{d+1}} \right], \quad d = 1, 2, \dots, D-1.$$

In addition to the ilr transformation, there are two other popular ways of representing elements of the simplex: additive log-ratio transformation (alr) and centered log-ratio transformation (clr) (Aitchison and Lauder, 1985). We focus on ilr coordinates, and from now on, for simplicity, when we refer to the ilr representation, we specifically refer to the isometry defined by Equation 10. It is important to emphasize that the methods described in this work are valid under any ilr transformation.

3.3. *Moments of simplicial statistics.* When addressing random compositions within a simplex, it is necessary to define certain key concepts. These include, among others, the identification of the center and the variance of a random composition. As shown in [Egozcue and Pawlowsky-Glahn \(2011\)](#), the center of a random composition  $\mathbf{y}$  can be defined as:

$$(11) \quad \text{Cen}(\mathbf{y}) = \text{ilr}^{-1} \mathbb{E}(\text{ilr}(\mathbf{y})) = \mathcal{C}(\exp(\mathbb{E}(\log(\mathbf{y})))) ,$$

where  $\mathbb{E}(\cdot)$  denotes the ordinary expectation in the ordinary real Euclidean space. Regarding the second order moments, a common metric for total variance of a random composition is defined as

$$(12) \quad \text{Var}_{\text{Tot}}(\mathbf{y}) = \mathbb{E}(d_a^2(\mathbf{y}, \text{Cen}(\mathbf{y}))) .$$

However, this is not the only way to express the total variance of a random composition. It can also be reformulated as the variance decomposition of the ilr coordinates, i.e.,

$$(13) \quad \text{Var}_{\text{Tot}}(\mathbf{y}) = \sum_{d=1}^{D-1} \text{Var}(y_d^*) ,$$

where  $y_d^*$  denotes the  $d$ th-coordinate of the random composition  $\mathbf{y}$ . As proved in [Egozcue and Pawlowsky-Glahn \(2005\)](#), the decomposition holds when the Aitchison distance is expressed in terms of orthonormal coordinates. The second-order structure is completed by the covariances between coordinates  $\text{Cov}(y_j^*, y_d^*)$  arranged in the  $(j, d)$ -entry of the  $(D-1) \times (D-1)$  covariance matrix  $\Sigma$  associated with the ilr coordinates.

#### 4. Bayesian Spatial Generalized Additive Models for CoDA.

4.1. *The simplicial regression.* Any kind of regression is primarily evaluated by its residuals. In the literature, in the context of CoDa, different assumptions have been proposed for modeling residuals. The most popular are the assumption of Dirichlet residuals or logistic-normal residuals. In this work, we focus on the logistic-normal distribution introduced by [Aitchison and Shen \(1980\)](#). They claim that if  $\mathbf{y} \in \mathcal{S}^D$ , whose representation in coordinates with respect to a selected orthonormal basis is  $\mathbf{y}^* \in \mathbb{R}^{D-1}$ ,  $\mathbf{y}^* = \text{ilr}(\mathbf{y})$ , the random composition  $\mathbf{y}$  has a logistic-normal distribution or, equivalently, a normal distribution in the simplex, whenever  $\mathbf{y}^*$  has a multivariate normal distribution, i.e.,  $\mathbf{y}^* \sim \mathcal{N}(\boldsymbol{\mu}, \Sigma)$ .

Once the ilr transformation has been applied, the compositional constraint which characterizes the CoDa is removed and multivariate Gaussian regression techniques can be applied to deal with them. Then, each mean of the transformed compositional coordinate ( $y_d^*$ ,  $d = 1, \dots, D-1$ ) is modeled as a function of covariates and other terms. If  $y_{\bullet n}^*$  denotes the  $(D-1)$ -dimensional  $n$ th vector of transformed observations ( $n = 1, \dots, N$ ), then the model is easily defined as

$$(14) \quad \begin{aligned} \mathbf{y}_{\bullet n}^* &\sim \mathcal{N}(\boldsymbol{\mu}_{\bullet n}, \Sigma) , \\ \mu_{dn} &= \eta_{dn}, \quad d = 1, \dots, D-1, \quad n = 1, \dots, N, \end{aligned}$$

where  $\Sigma$  is the variance-covariance matrix formed by the variances in the diagonal  $\Sigma_{dd} = \sigma_d^2$ ,  $d = 1, \dots, D-1$ , and covariances  $\Sigma_{dk} = \rho_{kd} \sigma_k \sigma_d$ , for  $k, d = 1, \dots, D-1$ , and  $k \neq d$ .  $\eta_{dn}$  denotes the linear predictor associated with the  $d$ th coordinate of the  $n$ th observation.

Once we are in the ordinary real Euclidean space, we deal with a multivariate Gaussian likelihood, which, as a member of the exponential family, allows the linear predictor to include different terms such as linear terms, spatial components, splines, etc. Finally, the inverse ilr transformation is applied to reconstruct compositions in  $\mathcal{S}^D$  from the fitted coordinates ([Pawlowsky-Glahn and Egozcue, 2016](#)). In the next section, we provide the multivariate model for extending the linear predictor within a GAM framework.

4.2. *Bayesian Generalized Additive models.* GAMs are flexible models that allow for the incorporation of linear and nonlinear effects in a regression framework for a response variable ( $Y_n$ ) in the exponential family (Hastie and Tibshirani, 1990). A common formulation is:

$$(15) \quad \eta_n = g(\mu_n) = \mathbf{X}_n \boldsymbol{\beta} + \sum_{j=1}^J f_j(x_{jn}),$$

where  $\mu_n = \mathbb{E}(Y_n)$ ,  $\mathbf{X}_n$  is the  $n$ th row of the design matrix for strictly parametric components of the model,  $\boldsymbol{\beta}$  is the corresponding parameter vector, and  $f_j$  are smooth functions of the covariates  $x_j$ , typically univariate, although multivariate smooths are also possible.

Bivariate smoothing plays a crucial role in fields such as epidemiology and ecology, particularly when dealing with georeferenced data. In these contexts, geostatistical methods like kriging are commonly applied, and they are closely related to spline-based approaches, including P-splines. Although spatial applications are a primary motivation in this work, bivariate smoothing is not limited to spatial data; it is also useful for capturing nonlinear relationships between any pair of continuous covariates. The recent widespread use of GAMs stems from advances in low-rank spline-based basis functions, such as thin plate splines and B-spline bases. However, P-splines remain a particularly effective and versatile smoothing tool, offering computational efficiency and flexibility (Eilers and Marx, 2021). In this work, we adopt on P-spline bases, as they provide a practical balance between model interpretability and performance.

As we are working in a Bayesian context, prior distributions for parameters of the model have to be established. In line with the R-package `brms`, whose main strategy to compute posterior distributions is the Hamiltonian Monte Carlo (HMC) method, we set priors for the fixed effects to zero-centered Gaussian prior with standard deviation 10, half Student- $t$  prior with 3 degrees of freedom for standard deviations and LKJ with regularization parameter set to 1 for correlation matrix (Bürkner, 2017). Finally, we can include a GAM in the context of CoDA. We model each ilr coordinate with its own linear predictor of the form given in Equation 15:

$$(16) \quad \begin{aligned} \mathbf{y}_{\bullet n}^* &\sim \mathcal{N}(\boldsymbol{\mu}_{\bullet n}, \boldsymbol{\Sigma}) \\ \mu_{dn} &= \mathbf{X}_n \boldsymbol{\beta}^d + \sum_{j=1}^{J^d} f_j^d(x_{jn}). \end{aligned}$$

**5. Bayesian model selection and Validation.** This section is devoted to introduce some measures to compare Bayesian additive models. In particular, we focus on WAIC (Gelman, Hwang and Vehtari, 2014) and the Bayesian  $R^2$  (Gelman et al., 2019).

5.1. *Watanabe-Akaike information criterion (WAIC).* WAIC is a fully Bayesian approach which has proven to be a reliable approximation for estimating the out-of-sample expectation. It is based on the computation of the log pointwise posterior predictive density ( $lppd$ ), along with a correction for the effective number of parameters ( $p_{\text{WAIC}}$ ) to adjust for model complexity (Gelman, Hwang and Vehtari, 2014; Vehtari, Gelman and Gabry, 2017). WAIC is defined as

$$(17) \quad \text{WAIC} = -2lppd + 2p_{\text{WAIC}},$$

being  $lppd = \sum_{n=1}^N \log \left( \frac{1}{S} \sum_{s=1}^S p(y_n | \theta^s) \right)$ , and  $p_{\text{WAIC}} = \sum_{n=1}^N V_{s=1}^S (\log(p(y_n | \theta^s)))$ . A lower WAIC indicates a better model fit, adjusted for model complexity. Note that we follow

the notation from [Gelman et al. \(2019\)](#), where  $V$  denotes the sample variance of any vector  $\mathbf{z} = (z_1, \dots, z_J)$ , defined as:

$$V_{j=1}^J z_j = \frac{1}{J-1} \sum_{j=1}^J (z_j - \bar{z})^2, \quad \text{with } \bar{z} = \frac{1}{J} \sum_{j=1}^J z_j.$$

**5.2. Bayesian  $R^2$ .** The coefficient of determination,  $R^2$ , is a widely used measure of goodness of fit that quantifies the proportion of variability in the response explained by the predictors. Classically, it is defined as the ratio between the variance of the predicted values and the total variance of the observed data. However, in Bayesian models, this definition presents a drawback: the variance of the predicted values can sometimes exceed the total variance of the data, which can result in  $R^2 > 1$ . [Gelman et al. \(2019\)](#) addressed this issue by proposing a Bayesian  $R^2$  that is well-defined based on the distribution of future data ( $y_n$ ) and the expected values conditional on the unknown parameters  $y_n^{\text{pred}} = \mathbb{E}(y_n | X_n, \theta)$ . Here,  $X_n$  denotes the set of predictors associated with  $y_n$ . For a linear model,  $y_n^{\text{pred}}$  corresponds to the linear predictor, while for a generalized linear model, it is the linear predictor transformed to the data scale. The Bayesian  $R^2$  is then defined as

$$(18) \quad R^2 = \frac{\text{Explained variance}}{\text{Explained variance} + \text{Residual variance}} = \frac{\text{var}_{fit}}{\text{var}_{fit} + \text{var}_{res}},$$

where  $\text{var}_{fit} = V_{n=1}^N \mathbb{E}(y_n | \theta) = V_{n=1}^N y_n^{\text{pred}}$  represents the variance of the predictive means, and  $\text{var}_{res} = \mathbb{E}(V_{n=1}^N (y_n - y_n^{\text{pred}}) | \theta)$  is the modeled residual variance. Both  $\text{var}_{fit}$  and  $\text{var}_{res}$  are defined conditionally on the model parameters  $\theta$ , therefore the resulting  $R^2$  is conditional on  $\theta$ . As discussed in [Gelman et al. \(2019\)](#), extending the definition of  $R^2$  to the Bayesian context simply requires acknowledging that inference is based on posterior simulation draws  $\theta^s$ , with  $s = 1, \dots, S$ . For each posterior draw  $\theta^s$ , the  $R^2$  can be computed as

$$(19) \quad R_s^2 = \frac{V_{n=1}^N y_n^{\text{pred},s}}{V_{n=1}^N y_n^{\text{pred},s} + \text{var}_{res}^s},$$

where  $y_n^{\text{pred},s} = \mathbb{E}(y_n | X_n, \theta^s)$  denotes the predictive mean for draw  $s$ , and  $\text{var}_{res}^s$  is the corresponding residual variance for that draw.

As discussed in [Vehtari et al. \(2025\)](#), there are two main approaches for defining the modeled residual variance in the Bayesian  $R^2$ . The first is the *residual-based* approach, which uses draws from the residual distribution and computes

$$(20) \quad \text{var}_{res}^s = V_{n=1}^N e_n^s,$$

where  $e_n^s = y_n - y_n^{\text{pred},s}$ .

The second is the *model-based* approach, which relies on draws from the modeled residual variances. For example, in linear regression,

$$(21) \quad \text{var}_{res}^s = (\sigma^2)^s,$$

while in logistic regression,

$$(22) \quad \text{var}_{res}^s = \frac{1}{N} \sum_{n=1}^N \pi_n^s (1 - \pi_n^s).$$

While in this work we follow the posterior-based formulation of  $R^2$  proposed by [Gelman et al. \(2019\)](#) and [Vehtari et al. \(2025\)](#), alternative approaches have emerged that leverage the same definition of  $R^2$  from a different perspective. For instance, [Zhang, Bondell and](#)

Reich (2020) and Aguilar and Bürkner (2023) propose placing prior distributions directly on the  $R^2$  coefficient as a means to construct informative priors on regression coefficients. These methods are primarily designed for prior specification and model regularization in high-dimensional or hierarchical settings, rather than as goodness-of-fit metrics. Although these perspectives are valuable in their own context, our focus here remains on the use of  $R^2$  as a posterior predictive measure for model evaluation.

**6. An extension of Bayesian  $R^2$  for CoDa.** We extend the concept of  $R^2$  to the CoDa context by grounding it in the total variability of a composition expressed through the variance decomposition of ilr coordinates (see Equation 13). This formulation, proposed by Egozcue and Pawlowsky-Glahn (2011), establishes the total variance as the sum of variances of the orthonormal ilr coordinates, thus fundamentally respecting the Aitchison geometry of the simplex. While this framework provides the core foundation for our CoDa- $R^2$ , related ideas were already explored by Hijazi and Jernigan (2009), who proposed alternative  $R^2$  measures grounded in compositional variance. Our proposal builds directly on the ilr-based decomposition, offering a natural extension to the Bayesian setting. Accordingly, the explained variability of CoDa can be expressed as the total variance of the predicted ilr coordinates:

$$(23) \quad \text{var}_{\text{fit}} = \sum_{d=1}^{D-1} V_{n=1}^N \left( y_{dn}^{*,\text{pred}} \right),$$

where  $y_{dn}^{*,\text{pred}}$  denotes the expected value of the  $d$ th ilr coordinate for the  $n$ th observation, conditional on the covariates  $X_n$  and the model parameters:

$$(24) \quad y_{dn}^{*,\text{pred}} = \mathbb{E} \left( y_{dn}^* \mid X_n, \theta \right).$$

As in the univariate case described by Gelman et al. (2019), bringing this definition to the Bayesian context involves computing the CoDa- $R^2$  for each posterior draw  $\theta^s$ , with  $s = 1, \dots, S$ . For each draw, the CoDa- $R^2$  is given by

$$(25) \quad \text{CoDa-}R_s^2 = \frac{\sum_{d=1}^{D-1} V_{n=1}^N \left( y_{dn}^{*,\text{pred},s} \right)}{\sum_{d=1}^{D-1} V_{n=1}^N \left( y_{dn}^{*,\text{pred},s} \right) + \text{var}_{\text{res}}^s},$$

where  $y_{dn}^{*,\text{pred},s} = \mathbb{E} \left( y_{dn}^* \mid X_n, \theta^s \right)$  represents the predictive mean of the  $d$ th ilr coordinate for observation  $n$  at posterior draw  $s$ . In line with Gelman et al. (2019) and Vehtari et al. (2025), we consider two alternative formulations for  $\text{var}_{\text{res}}^s$ :

1. *Residual-based CoDa- $R^2$  (BR-CoDa- $R^2$ ):*

$$(26) \quad \text{var}_{\text{res}}^s = \sum_{d=1}^{D-1} V_{n=1}^N \left( y_{dn}^{*,s} - y_{dn}^{*,\text{pred},s} \right),$$

where  $y_{dn}^{*,s}$  is the observed ilr coordinate.

2. *Model-based CoDa- $R^2$  (BM-CoDa- $R^2$ ):*

$$(27) \quad \text{var}_{\text{res}}^s = \sum_{d=1}^{D-1} \Sigma_{dd}^s,$$

where  $\Sigma_{dd}^s$  denotes the posterior draw of the variance of the  $d$ th ilr coordinate.

Both formulations provide coherent, geometry-respecting measures of explained variability for CoDa models, fully compatible with the Bayesian paradigm. In what follows, we demonstrate how these measures can guide model comparison and validation in practical applications.

CoDa- $R^2$  enables a principled quantification of the probability that one model explains more variability than another. The Bayesian framework naturally provides posterior distributions for CoDa- $R^2$ , making it straightforward to compute probabilities such as  $P(\text{CoDa-}R_{M1}^2 \geq \text{CoDa-}R_{M2}^2)$  when comparing two competing models, M1 and M2. By fixing the credible level at  $\alpha = 0.1$ , we consider a difference substantial if this probability exceeds  $1 - \alpha = 0.9$ , indicating that M1 explains substantially more variability than M2. If the probability is below  $\alpha = 0.1$ , we conclude that M2 explains substantially more variability than M1. Probabilities lying between 0.1 and 0.9 suggest that both models have a similar explanatory capacity. This threshold serves as a pragmatic decision rule rather than a formal hypothesis test, and the choice of  $\alpha$  corresponds to the level of uncertainty we are willing to tolerate in model comparison. This approach provides an intuitive and consistent basis for evaluating the relative explanatory capacity of competing models within a Bayesian framework.

Remark that this tool is particularly useful when comparing nested models, as it allows us to quantify how relevant the inclusion of a new variable is in explaining additional variability. Specifically, it provides a direct assessment of the proportion of variability accounted for by the new variable when added to the extended model. This makes CoDa- $R^2$  a powerful and interpretable metric for model selection, especially in applications involving compositional data.

**7. Simulation examples.** This section presents three simulation studies to evaluate the performance of the proposed methodology under controlled settings. The first example assesses the ability of a Bayesian linear CoDa model to recover the true parameters and hyperparameters. The second example evaluates the accuracy of CoDa regression when smooth terms are incorporated into the linear predictor, including both univariate and bivariate smooth components. The final example compares BM-CoDa- $R^2$  and BR-CoDa- $R^2$  for model discrimination under varying data-generating mechanisms.

*7.1. Bayesian CoDa linear regression.* The first simulation considers CoDa in  $\mathcal{S}^4$ . A sample of 100 realizations was drawn from a 3-dimensional Gaussian distribution with the following structure:

$$(28) \quad \begin{aligned} \mathbf{y}_{\bullet n}^* &\sim \mathcal{N}(\boldsymbol{\mu}_{\bullet n}, \boldsymbol{\Sigma}) \\ \mu_{dn} &= \beta_0^d + \beta_1^d x_{1n} + \beta_2^d x_{2n} + \beta_3^d x_{3n}. \end{aligned}$$

where  $x_{kn}$ ,  $k = 1, \dots, 3$ ,  $n = 1, \dots, 100$ , are covariates drawn independently from a Uniform(0, 1) distribution, and  $\beta_k^d$  are the fixed parameters corresponding to the  $d$ th ilr coordinate and the  $k$ th covariate, with  $k = 0$  denoting the intercept. The intercepts were fixed to  $\beta_0^1 = 1$ ,  $\beta_0^2 = -0.5$ , and  $\beta_0^3 = -2$ . For the slopes, we specified  $\beta_1^1 = -0.5$ ,  $\beta_2^1 = 1$ ,  $\beta_3^1 = -0.5$  for the first ilr coordinate;  $\beta_1^2 = 1$ ,  $\beta_2^2 = -1$ ,  $\beta_3^2 = 0$  for the second; and  $\beta_1^3 = 1$ ,  $\beta_2^3 = -0.5$ ,  $\beta_3^3 = -0.5$  for the third. The standard deviations were fixed at  $\sigma_1 = 0.10$ ,  $\sigma_2 = 0.05$ , and  $\sigma_3 = 0.08$ , with correlation parameters  $\rho_{12} = 0.5$ ,  $\rho_{13} = 0.2$ , and  $\rho_{23} = 0.8$ . These small standard deviations reduce noise, facilitating the assessment of parameter recovery. After generating the data in  $\mathbb{R}^3$ , the inverse ilr transformation was applied to obtain simulated compositional data in  $\mathcal{S}^4$ .

Bayesian inference was conducted by assigning prior distributions to both regression coefficients and covariance parameters. Specifically, Gaussian priors with mean 0 and standard

deviation 10 were specified for the fixed effects. For the standard deviations, default priors were employed; in particular, a half Student- $t$  prior with 3 degrees of freedom and a scale parameter dependent on the standard deviation of the response after applying the link function. The correlation matrix was assigned a LKJ prior with regularization parameter set to 1. To demonstrate that the model is capable of recovering the true parameter values, Table 2 reports the posterior means and 95% credible intervals for the fixed effects, standard deviations, and correlations. In all cases, the true values lie within the corresponding 95% credible intervals.

TABLE 2  
Means and 95% credible intervals for the sample posterior distributions. Comparison with real values.

		Fixed effects				
ilr coordinate	Parameter	Real value	Mean	Q 2.5%	Q 97.5%	
First	$\beta_0$	1.000	0.896	0.449	1.370	
	$\beta_1$	-0.500	-0.479	-0.499	-0.457	
	$\beta_2$	1.000	0.993	0.965	1.023	
	$\beta_3$	-0.500	-0.506	-0.527	-0.484	
Second	$\beta_0$	-0.500	-0.543	-0.730	-0.357	
	$\beta_1$	1.000	0.998	0.989	1.007	
	$\beta_2$	-1.000	-1.000	-1.012	-0.989	
	$\beta_3$	0.000	0.006	-0.003	0.015	
Third	$\beta_0$	-2.000	-1.981	-2.278	-1.676	
	$\beta_1$	1.000	0.993	0.979	1.006	
	$\beta_2$	-0.500	-0.504	-0.523	-0.486	
	$\beta_3$	-0.500	-0.491	-0.504	-0.477	
		Hyperparameters				
	Parameter	Real value	Mean	Q 2.5%	Q 97.5%	
	$\sigma_1$	0.100	0.108	0.094	0.125	
	$\sigma_2$	0.050	0.045	0.039	0.051	
	$\sigma_3$	0.080	0.070	0.061	0.081	
	$\rho_{12}$	0.500	0.554	0.403	0.679	
	$\rho_{13}$	0.200	0.252	0.061	0.426	
	$\rho_{23}$	0.800	0.786	0.699	0.853	

Model fit was further assessed by comparing posterior predictive distributions with the original data. This visualization allows for a direct comparison between the predicted compositions and the true values, providing an intuitive validation of the model fit. Further details can be found in Figure 11 (Appendix).

7.2. *Bayesian CoDa GAM.* This second example considers CoDa in  $\mathcal{S}^3$ . A total of 100 realizations were generated from a bivariate Gaussian distribution with the following structure:

$$(29) \quad \mathbf{y}_{\bullet n}^* \sim \mathcal{N}(\boldsymbol{\mu}_{\bullet n}, \boldsymbol{\Sigma}),$$

$$\mu_{dn} = f_1^d(x_{s_{1n}}) + f_2^d(x_{s_{2n}}, x_{s_{3n}}),$$

where  $f_1^d(x_{s_{1n}})$  denotes a univariate smooth function for the  $d$ th ilr coordinate and covariate  $x_{s_{1n}}$  in the  $n$ th observation, and  $f_2^d(x_{s_{2n}}, x_{s_{3n}})$  denotes a bivariate smooth function for the  $d$ th ilr coordinate and covariates  $x_{s_{2n}}$  and  $x_{s_{3n}}$ . The covariates  $x_{s_{kn}}$ , with  $k = 1, \dots, 3$ , were simulated from a Uniform(0, 1) distribution. The functions were defined as

$$(30) \quad f_1^1(x_{s_1}) = 0.2x_{s_1}^{11}(10(1-x_{s_1}))^6$$

$$+ 10(10x_{s_1})^3(1-x_{s_1})^{10},$$

$$(31) \quad f_1^2(x_{s_1}) = \sin(2\pi x_{s_1}).$$

It is worth noting that Equation 30 corresponds to one of the components of the classic four-term additive model introduced by Gu and Wahba (1991), widely used as a benchmark for testing smooth term recovery. It was simulated using the function `gamSim` from the R package `mgcv` (Wood, 2017). The same R package was used to simulate two bivariate smooth functions:

$$(32) \quad f_2^1(x_{s_2}, x_{s_3}) = (\pi^{0.3} 0.4) \left( 1.2 \exp \left( -\frac{(x_{s_2} - 0.2)^2}{0.3^2} - \frac{(x_{s_3} - 0.3)^2}{0.4^2} \right) + 0.8 \exp \left( -\frac{(x_{s_2} - 0.7)^2}{0.3^2} - \frac{(x_{s_3} - 0.8)^2}{0.4^2} \right) \right),$$

$$(33) \quad f_2^2(x_{s_2}, x_{s_3}) = (\pi^{0.3} 0.4) 1.2 \exp \left( -\frac{(x_{s_2} - 0.5)^2}{0.3^2} - \frac{(x_{s_3} - 0.5)^2}{0.4^2} \right).$$

All functions were subsequently centered. The standard deviations and correlation parameter were set to 0.05, 0.03, and 0.5, respectively. Finally, applying the inverse `ilr` transformation allowed us to map the data to  $\mathcal{S}^3$  (see Figure 2). The main objective of this example is to reconstruct the nonlinear functions.

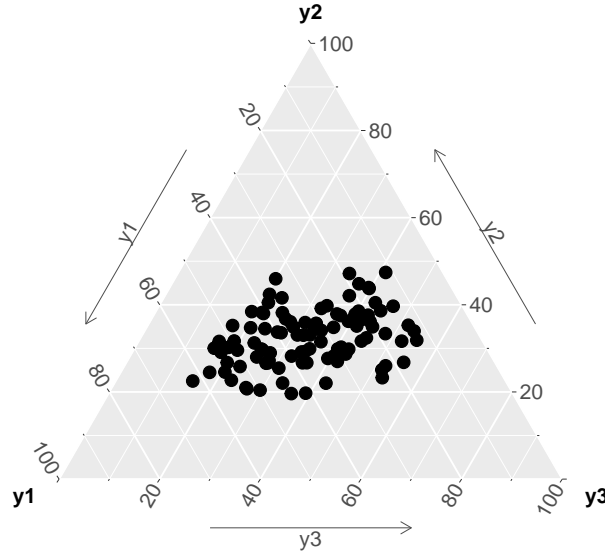


FIG 2. Simulated data in  $\mathcal{S}^3$ . The composition is represented in percentages.

For inference, we adopted the same functional structure as in the data-generating mechanism, replacing  $f_1^d(\cdot)$  with  $s^d(\cdot)$  to represent univariate penalized P-splines, and  $f_2^d(\cdot)$  with  $t^d(\cdot)$  to denote tensor-product smooths based on P-spline bases. Gaussian priors with mean zero and standard deviation 10 were specified for the smooth coefficients. For the standard deviations and correlation matrix, we again used default priors: specifically, a half-Student- $t$  distribution with 3 degrees of freedom for the standard deviations, and a LKJ prior with regularization parameter set to 1 for the correlation matrix.

The fitted model successfully recovers the underlying smooth effects, as illustrated in Figure 3 and Figure 4. Additionally, Figure 5 shows the posterior distributions of the standard

deviations and correlation parameter, confirming that the true values are well captured by the model.

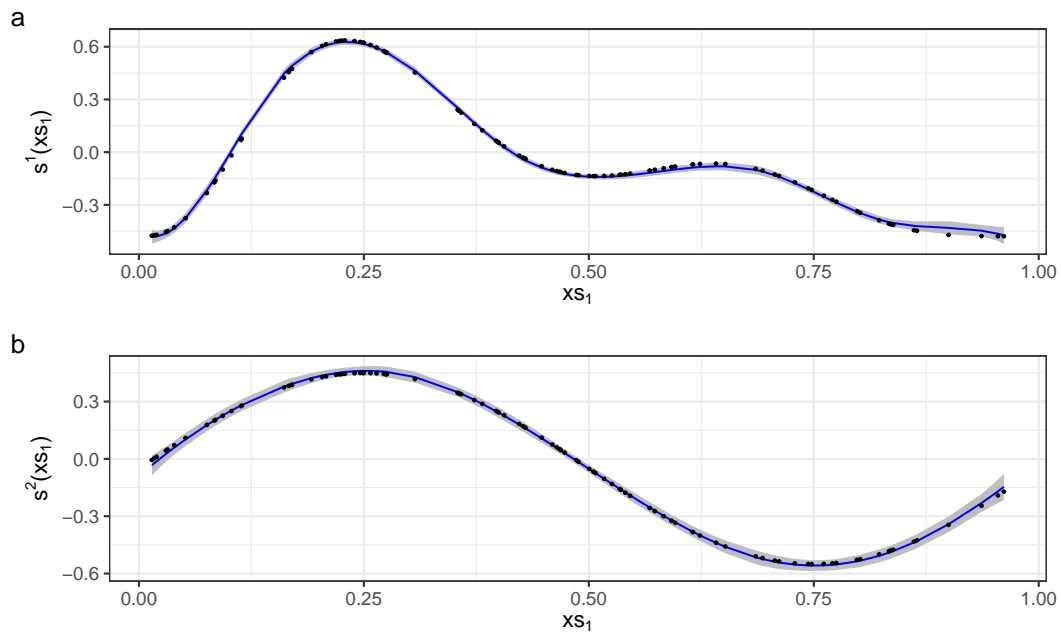


FIG 3. Points represent the simulated data from the one-dimensional smooth functions  $f_1^d$ , with  $d = 1, 2$ . The blue lines and gray regions correspond to the posterior mean and the 95% credible intervals, respectively, for the estimated smooth terms  $s^d(x_{S_1})$ , with  $d = 1, 2$ .

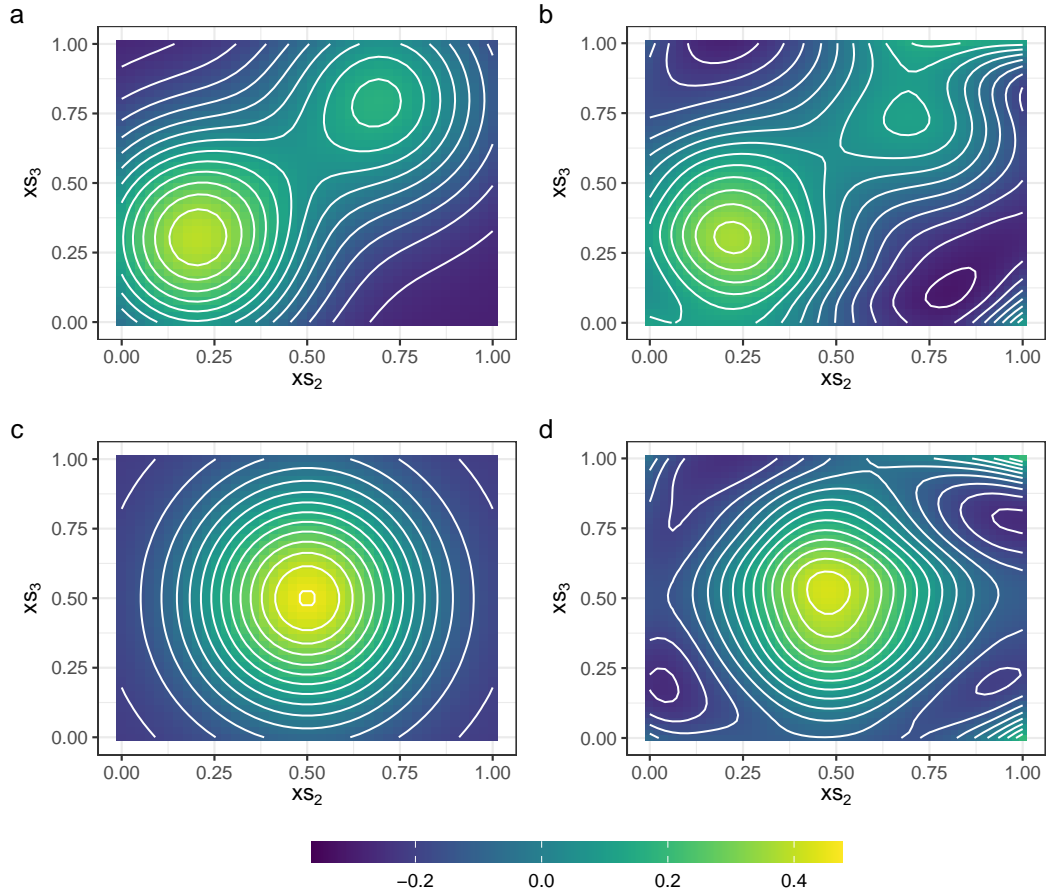


FIG 4. (a) and (c) Contour plots of the simulated bivariate smooth functions  $f_2^1$  and  $f_2^2$ . (b) and (d) Posterior mean estimates of the smooth terms  $t^1(x_{s2}, x_{s3})$  and  $t^2(x_{s2}, x_{s3})$ , respectively.

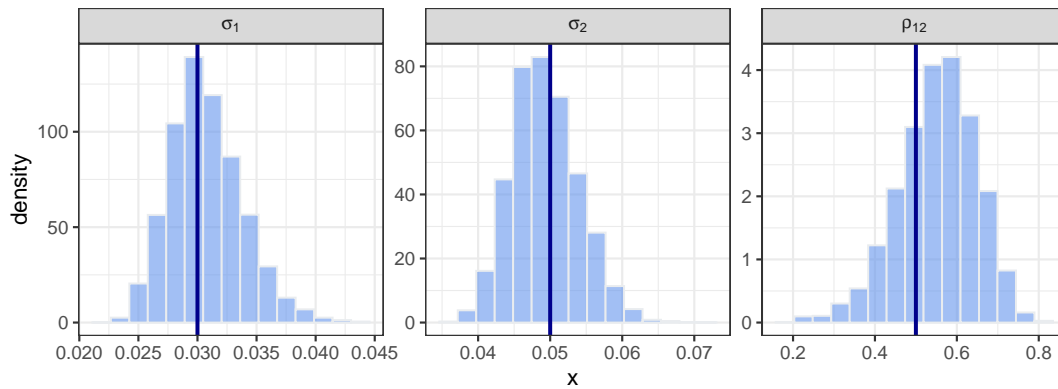


FIG 5. Histograms with the posterior distribution for the standard deviations  $\sigma_1$  and  $\sigma_2$ , and the correlation parameter  $\rho_{12}$ . Vertical lines correspond with the real values from the simulation.

To further assess the performance of the model, we also represented the mean posterior predictive distribution alongside the original data. This visualization illustrates how well the model recovers the true underlying compositional structure in the simplex after applying the inverse ilr transformation. The plot provided in [Figure 12](#) (Appendix) offers a clear diagnostic of the predictive fit, confirming the model's ability to accurately capture the complex nonlinear relationships present in the simulated data.

*7.3. Model Comparison Using CoDa- $R^2$ .* Using the simulated data and model structures described in [Equation 28](#) and [Equation 29](#), we fitted several models and computed WAIC along with our proposed measures: BR-CoDa- $R^2$  and BM-CoDa- $R^2$ . In the linear regression case, we generated an additional covariate,  $x_4$ , which was not involved in the data-generating process. This allowed us to evaluate the behavior of our proposed measures in the presence of an irrelevant covariate. In the GAM case, no additional covariates were included; instead, we assessed model flexibility by varying the number of spline basis functions (5 and 10 nodes). Increasing the number of nodes results in greater model flexibility and more complex spline shapes. [Table 3](#) summarizes the predictors used in each model for both the linear regression and GAM settings, along with the corresponding WAIC values and posterior means (and standard deviations) of BR-CoDa- $R^2$  and BM-CoDa- $R^2$ .

TABLE 3  
Linear predictors for the different models where WAIC and the Bayesian CoDa- $R^2$  were computed. WAIC and mean (standard deviation) of the posterior distribution of BR-CoDa- $R^2$  and BM-Coda- $R^2$  are presented.

Linear regression				
Code	Model	WAIC	BR-CoDa- $R^2$	BM-CoDa- $R^2$
M1	$\beta_0^d + \beta_1^d x_{1n} + \beta_2^d x_{2n} + \beta_3^d x_{3n}$	-884.760	0.996 (0.001)	0.996 (0.001)
M2	$\beta_0^d + \beta_1^d x_{1n} + \beta_2^d x_{2n} + \beta_4^d x_{4n}$	-324.312	0.890 (0.003)	0.888 (0.010)
M3	$\beta_0^d + \beta_1^d x_{1n} + \beta_2^d x_{2n}$	-329.142	0.891 (0.003)	0.889 (0.011)
M4	$\beta_0^d + \beta_1^d x_{1n}$	277.355	0.567 (0.033)	0.562 (0.039)
M5	$\beta_0^d + \beta_2^d x_{2n}$	326.609	0.424 (0.046)	0.420(0.050)
M6	$\beta_0^d + \beta_4^d x_{4n}$	430.729	0.011 (0.012)	0.011 (0.012)
GAM				
Code	Model	WAIC	BR-CoDa- $R^2$	BM-CoDa- $R^2$
M1	$s^d(x_{s_{1n}}, k = 10) + t^d(x_{s_{2n}}, x_{s_{3n}}, k = 10)$	-690.713	0.989 (0.001)	0.989 (0.002)
M2	$s^d(x_{s_{1n}}, k = 5) + t^d(x_{s_{2n}}, x_{s_{3n}}, k = 5)$	-416.114	0.950 (0.004)	0.948 (0.006)
M3	$t^d(x_{s_{2n}}, x_{s_{3n}}, k = 10)$	87.851	0.264 (0.048)	0.261 (0.050)
M4	$t^d(x_{s_{2n}}, x_{s_{3n}}, k = 5)$	101.225	0.222 (0.048)	0.219 (0.050)
M5	$s^d(x_{s_{1n}}, k = 10)$	-99.864	0.779 (0.016)	0.773 (0.022)
M6	$s^d(x_{s_{1n}}, k = 5)$	-80.950	0.756 (0.018)	0.750 (0.023)

As expected, the results of BR-CoDa- $R^2$  and BM-CoDa- $R^2$  (see [Table 3](#)) indicate that models including all the terms used in the data-generating process explain a larger proportion of the variability, in agreement with the WAIC results. In the linear CoDa regression setting, model M1 achieves the best overall fit according to both WAIC and CoDa- $R^2$ . We computed the probabilities  $P(\text{CoDa-}R^2_{M_1} \geq \text{CoDa-}R^2_{M_j})$  for  $j = 2, \dots, 6$ , using both BR-CoDa- $R^2$  and BM-CoDa- $R^2$ . In all cases, these probabilities were equal to 1, indicating that M1 consistently explains more variability than any of the other models. In contrast, model M6, which included a covariate irrelevant to the data-generating process, shows the weakest

performance. We also computed WAIC and the probabilities  $P(\text{CoDa-}R_{M6}^2 \geq \text{CoDa-}R_{M_j}^2)$  for  $j = 1, \dots, 5$ , which were equal to 0 in all cases. These results confirm that M6 explains significantly less variability than the other models. Models M2 and M3 account for similar amounts of variability: the probabilities  $P(\text{CoDa-}R_{M2}^2 \geq \text{CoDa-}R_{M3}^2)$  were 0.424 for BR-CoDa- $R^2$  and 0.477 for BM-CoDa- $R^2$ , suggesting no relevant difference in the variability explained by both models.

Additionally, the nested structure of the models allows us to assess the contribution of individual covariates in terms of explained variability, and to determine their relevance. For instance, in the linear regression example from [Table 3](#), M3 is nested within both M1 and M2. Therefore, we can evaluate the relevance of adding variable  $x_1$  (in M1) or  $x_4$  (in M2) to M3, and quantify the additional variability explained by each.

Adding  $x_3$  to model M3 yields model M1. The probability  $P(\text{CoDa-}R_{M1}^2 \geq \text{CoDa-}R_{M3}^2)$  was 1 for both BR-CoDa- $R^2$  and BM-CoDa- $R^2$ , indicating that M1 explains substantially more variability than M3. On average,  $x_3$  contributes approximately a 10% increase in explained variability compared to M3. In contrast, adding  $x_4$  to M3 results in model M2. The  $P(\text{CoDa-}R_{M2}^2 \geq \text{CoDa-}R_{M3}^2)$  is 0.424 for BR-CoDa- $R^2$  and 0.477 for BM-CoDa- $R^2$ , indicating no relevant difference in explained variability. Consequently, the simpler model, M3, is preferred.

In the GAM case, model M1, which includes both univariate and bivariate smooth terms with 10 basis functions for  $xs_1$ ,  $xs_2$ , and  $xs_3$ , explains substantially more variability than the other models, as the  $P(\text{CoDa-}R_{M1}^2 \geq \text{CoDa-}R_{M_j}^2)$ ,  $j = 2, \dots, 6$  is 1. This is consistent with the WAIC results. On the other hand, models including only the bivariate smooth terms (M3 and M4) explain the least variability. The resulting probabilities,  $P(\text{CoDa-}R_{M3}^2 \geq \text{CoDa-}R_{M4}^2)$ , are 0.730 for BR-CoDa- $R^2$  and 0.707 for BM-CoDa- $R^2$ . Thus, we conclude that both models explain a similar amount of variability, and that the impact of covariates  $xs_2$  and  $xs_3$  on the response variable is lower than that of  $xs_1$ . As in the linear CoDa regression case, the nested structure of models M3 and M5 within M1, and M4 and M6 within M2, allows us to quantify the variability explained by each term when transitioning from M3 or M5 to M1, or from M4 or M6 to M2. Lastly, in line with the univariate proposal by [Vehtari et al. \(2025\)](#), we also observed that the distribution of BR-CoDa- $R^2$  remains narrower than that of BM-CoDa- $R^2$ .

**8. A Bayesian CoDa-GAM for soil texture prediction in the Basque Country.** Let  $\mathbf{y}_{\bullet n}$  be a 3-dimensional compositional vector representing the proportions of sand ( $y_{1n}$ ), silt ( $y_{2n}$ ), and clay ( $y_{3n}$ ). The model under study is then defined as

$$(34) \quad \begin{aligned} \mathbf{y}_{\bullet n}^* &= \text{ilr}(\mathbf{y}_{\bullet n}) \sim \mathcal{N}(\boldsymbol{\mu}_{\bullet n}, \boldsymbol{\Sigma}), \\ \mu_{dn} &= \beta_0^d + \beta_1^d \text{Lit}_n + \beta_2^d \text{Year}_n + s_1^d(\text{Elev}_n) + s_2^d(\text{Slope}_n) + t^d(\text{Lon}_n, \text{Lat}_n), \end{aligned}$$

where  $\mathbf{y}_{\bullet n}^* = [y_{1n}^*, y_{2n}^*]$  is the 2-dimensional ilr coordinate vector of the  $n$ th observation. The ilr coordinates correspond to the following balance-based representation (see [Equation 10](#)):

$$(35) \quad \begin{aligned} y_{1n}^* &= \sqrt{\frac{1}{2}} \log \left( \frac{y_{1n}}{y_{2n}} \right), \\ y_{2n}^* &= \sqrt{\frac{2}{3}} \log \left( \frac{(y_{1n}y_{2n})^{1/2}}{y_{3n}} \right). \end{aligned}$$

We note that the first ilr coordinate quantifies the relative proportion of sand to silt, whereas the second ilr coordinate measures the balance between the geometric mean of sand and silt relative to clay.  $\text{Lit}_n$  (Lithology) is modeled as a fixed effect,  $\text{Year}_n$  (Year) as a random effect,  $s^d(\bullet)$  denotes a univariate penalized P-spline, and  $t^d(\bullet)$  represents a bivariate tensor

product in a penalized P-spline basis. Priors for the model parameters were set to Gaussian distributions centered at 0 with a standard deviation of 10. Default priors were assigned for the standard deviations (half Student- $t$  prior with 3 degrees of freedom) and for the correlation matrix (LKJ prior with regularization parameter equal to 1). Model comparison was based on WAIC and the proposed Bayesian CoDa- $R^2$  measures, which were used to assess goodness of fit and guide model selection.

8.1. *Model comparison.* We compared several candidate models using WAIC, BR-CoDa- $R^2$ , and BM-CoDa- $R^2$  (see Table 4 and Figure 6). Model M1, which includes spatial effects (longitude and latitude), Lithology, Elevation, Slope, and a random Year effect, achieved the best balance between model fit and complexity, as evidenced by the lowest WAIC value. It also explained the highest proportion of variability according to both BR-CoDa- $R^2$  and BM-CoDa- $R^2$ . The posterior probabilities  $P(\text{CoDa-}R^2_{M1} \geq \text{CoDa-}R^2_{M_j})$ ,  $j = 2, \dots, 5$ , were 0.969, 1, 1, and 1 for BR-CoDa- $R^2$ , and 0.957, 1, 1, and 1 for BM-CoDa- $R^2$ , confirming that M1 consistently outperformed the alternatives. Comparing M1 and M2 emphasizes the contribution of the random Year effect, which accounts for an average increase of approximately 3% in explained variability under both BR-CoDa- $R^2$  and BM-CoDa- $R^2$ . This highlights the relevance of accounting for inter-annual variability in soil texture modeling.

Overall, the results underscore the importance of including spatial effects and key covariates (such as lithology, elevation, and slope) to adequately capture soil texture composition. Models omitting these components (e.g., M4 and M5) showed a notable reduction in explanatory power, as reflected by both WAIC and CoDa- $R^2$ . Figure 6 illustrates how M1 achieved the highest mean CoDa- $R^2$ , supporting its suitability for our analysis.

TABLE 4

*Summary of the models fitted to the soil texture dataset. For each model, the WAIC and the posterior mean (with standard deviation) of the BR-CoDa- $R^2$  and BM-CoDa- $R^2$  are reported.*

Code	Lit	Elev	Slope	Lon, Lat	Year	WAIC	BR-CoDa- $R^2$	BM-CoDa- $R^2$
M1	✓	✓	✓	✓	✓	2369.722	0.346 (0.011)	0.346 (0.012)
M2	✓	✓	✓	✓	–	2607.442	0.315 (0.011)	0.315 (0.013)
M3	–	✓	✓	✓	–	2715.712	0.299 (0.012)	0.298 (0.013)
M4	–	–	–	✓	–	2773.772	0.284 (0.011)	0.284 (0.012)
M5	✓	–	–	–	–	3986.285	0.071 (0.007)	0.071 (0.008)

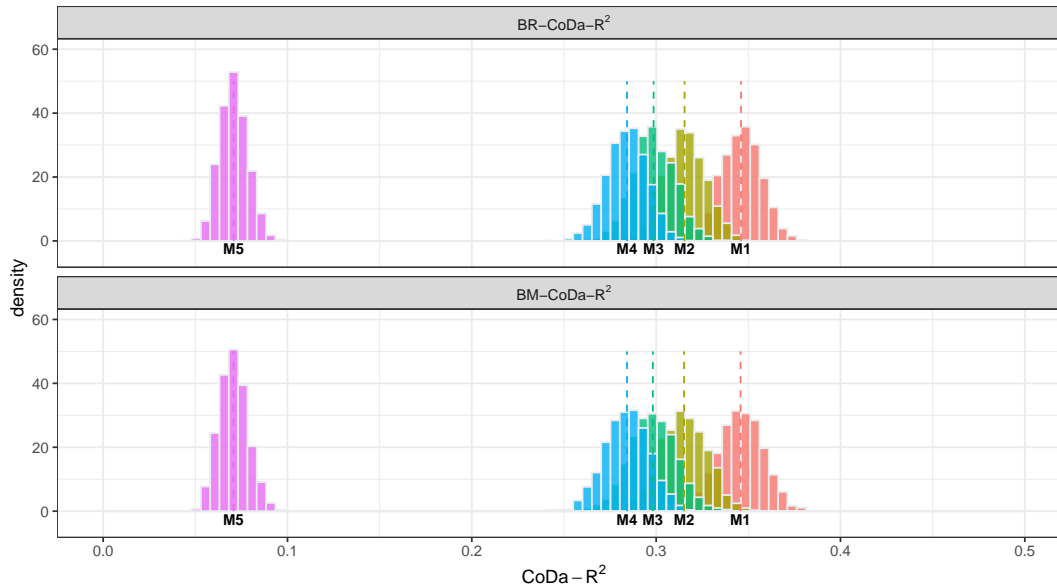


FIG 6. Posterior distributions of  $BR-CoDa-R^2$  and  $BM-CoDa-R^2$  for each of the soil texture models. Each bar summarizes the mean and variability in explained compositional variance across the different model specifications.

8.2. *Best model and predictions.* After selecting the best model to represent the process of interest, we computed the posterior distribution of the fixed effects and smooth terms. The `brms` package allowed us to obtain these in a straightforward way. Estimates were obtained in real space, the domain where inference is carried out. While fixed effects retain a direct interpretation in this space, smooth terms are more naturally understood in the original compositional space  $\mathcal{S}^3$ . Owing to the isometric property of the `ilr` transformation, it suffices to apply the inverse `ilr` transformation directly to the posterior simulations to recover results in the simplex.

In Table 5, we report the posterior distributions of the parameters corresponding to the fixed effect of Lithology. Category 1 (Surface deposits) serves as the reference level. For the first `ilr` coordinate, which quantifies the log-ratio between sand and silt, the largest positive contribution is associated with category 6 (Decarbonate marls). The posterior mean of the parameter indicates that, for decarbonate marls, the sand-to-silt ratio is on average 35% higher than in surface deposits. For the second `ilr` coordinate, which measures the balance between the geometric mean of sand and silt relative to clay, category 12 (Limestones and dolomites) shows the highest positive contribution. The posterior mean suggests that, under this lithology, the combined proportion of sand and silt relative to clay is on average 73% higher than in surface deposits.

Figure 7 and Figure 8 display the posterior marginal distributions of the smooth terms for slope and elevation. The plots reveal that increasing slope is associated with a higher proportion of clay and a lower proportion of sand and silt. Conversely, higher elevations correspond to a slight increase in sand and clay and a decrease in silt. Thanks to the Bayesian framework, we can quantify the associated uncertainty. Uncertainty in the slope effect is lower at higher slope values, and a similar pattern is observed for elevation, with reduced uncertainty around 500 meters.

The posterior distributions of the two-dimensional smooth spatial terms are shown in Figure 9. These plots reveal clear spatial patterns in the composition of sand, silt, and clay

TABLE 5  
*Posterior distribution of the parameters corresponding to the fixed effect Lithology. Category 1 (Surface deposits) serves as the reference level.*

Lithology	ilr1			ilr2		
	Mean	Q 2.5%	Q 97.5%	Mean	Q 2.5%	Q 97.5%
Lito2	0.005	-0.124	0.132	0.062	-0.119	0.233
Lito3	0.143	-0.104	0.373	-0.019	-0.334	0.305
Lito4	0.035	-0.129	0.193	0.117	-0.109	0.346
Lito5	0.042	-0.019	0.104	-0.063	-0.146	0.020
Lito6	0.302	0.099	0.492	0.175	-0.083	0.434
Lito7	0.158	0.088	0.224	0.193	0.100	0.286
Lito8	0.151	0.096	0.202	0.116	0.046	0.183
Lito9	-0.050	-0.126	0.028	0.228	0.125	0.333
Lito10	0.156	0.117	0.195	0.129	0.075	0.183
Lito11	0.022	-0.184	0.224	-0.020	-0.301	0.255
Lito12	0.008	-0.300	0.319	0.550	0.138	0.964
Lito13	-0.046	-0.180	0.089	0.150	-0.027	0.337

across the study region. For sand, higher proportions are predicted in specific geographic areas, likely corresponding to zones of lower elevation or particular lithologies. In contrast, silt shows increased proportions in areas where sand decreases, reflecting the natural balance in CoDa. Clay proportions appear more homogeneous across space, with no strong spatial gradient detected.

The Bayesian framework facilitates the joint visualization of spatial mean predictions and associated uncertainties. The credible intervals indicate that uncertainty is generally lower in regions with dense sampling and higher in peripheral or less-sampled areas.

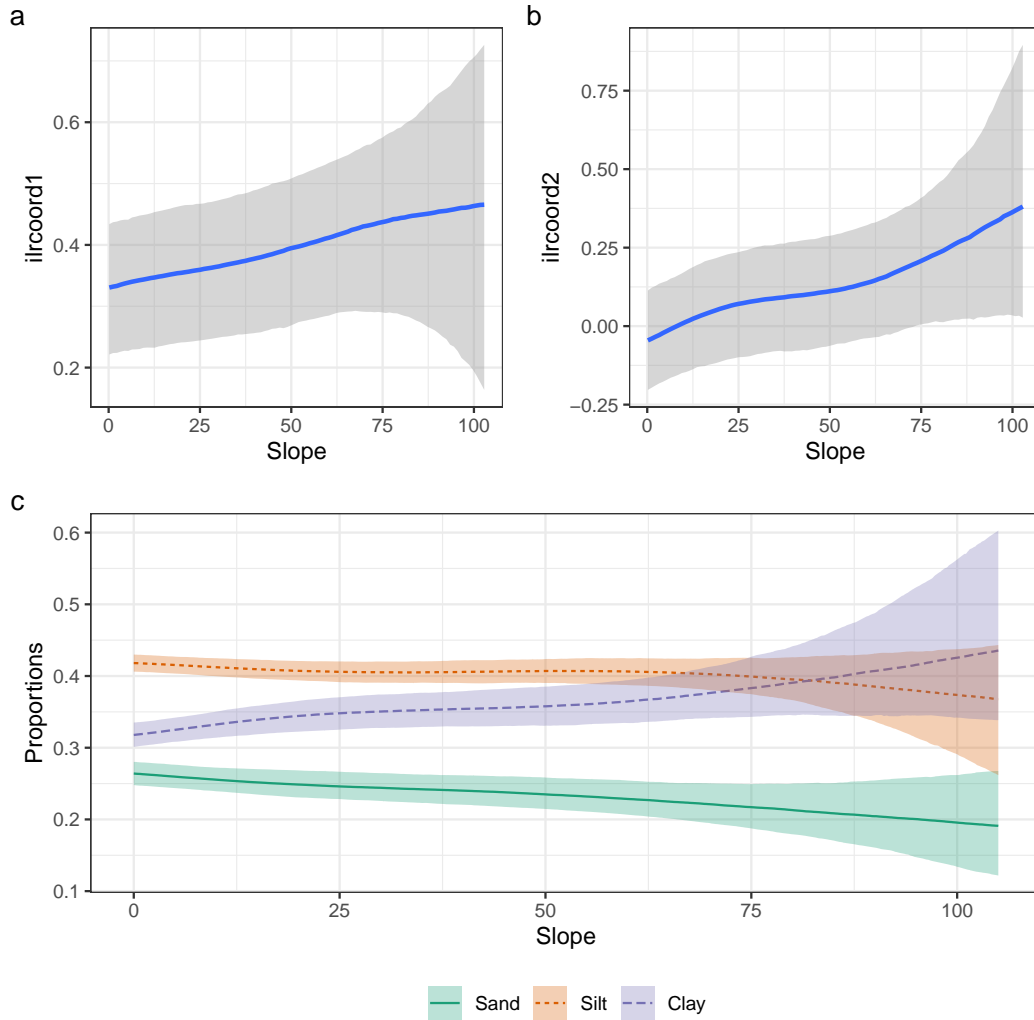


FIG 7. Marginal posterior distribution of the smooth effect of slope on the ilr-transformed soil texture coordinates and their transformation to the compositional space. Panel (a) shows the expected response of the first ilr coordinate as a smooth function of slope, and panel (b) shows the same for the second ilr coordinate. In both cases, all other covariates were fixed at reference values. Panel (c) displays the corresponding posterior distributions for the original soil composition (sand, silt, and clay) obtained by applying the inverse ilr transformation. Solid lines represent posterior medians and shaded bands represent 95% credible intervals.

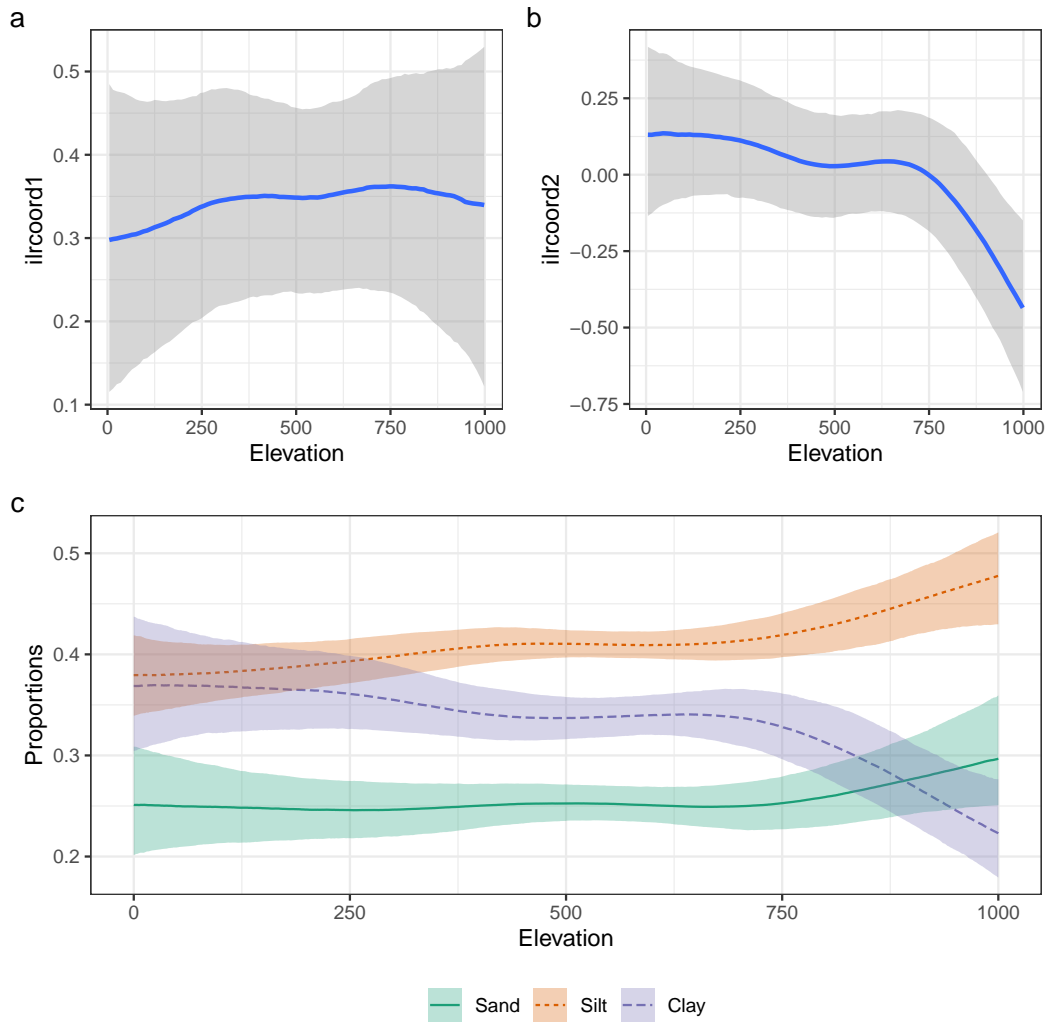


FIG 8. Marginal posterior distribution of the smooth effect of elevation on the ilr-transformed soil texture coordinates and their transformation to the compositional space. Panel (a) shows the expected response of the first ilr coordinate as a smooth function of elevation, and panel (b) shows the same for the second ilr coordinate. In both cases, all other covariates were fixed at reference values. Panel (c) displays the corresponding posterior distributions for the original soil composition (sand, silt, and clay) obtained by applying the inverse ilr transformation. Solid lines represent posterior medians and shaded bands represent 95% credible intervals.

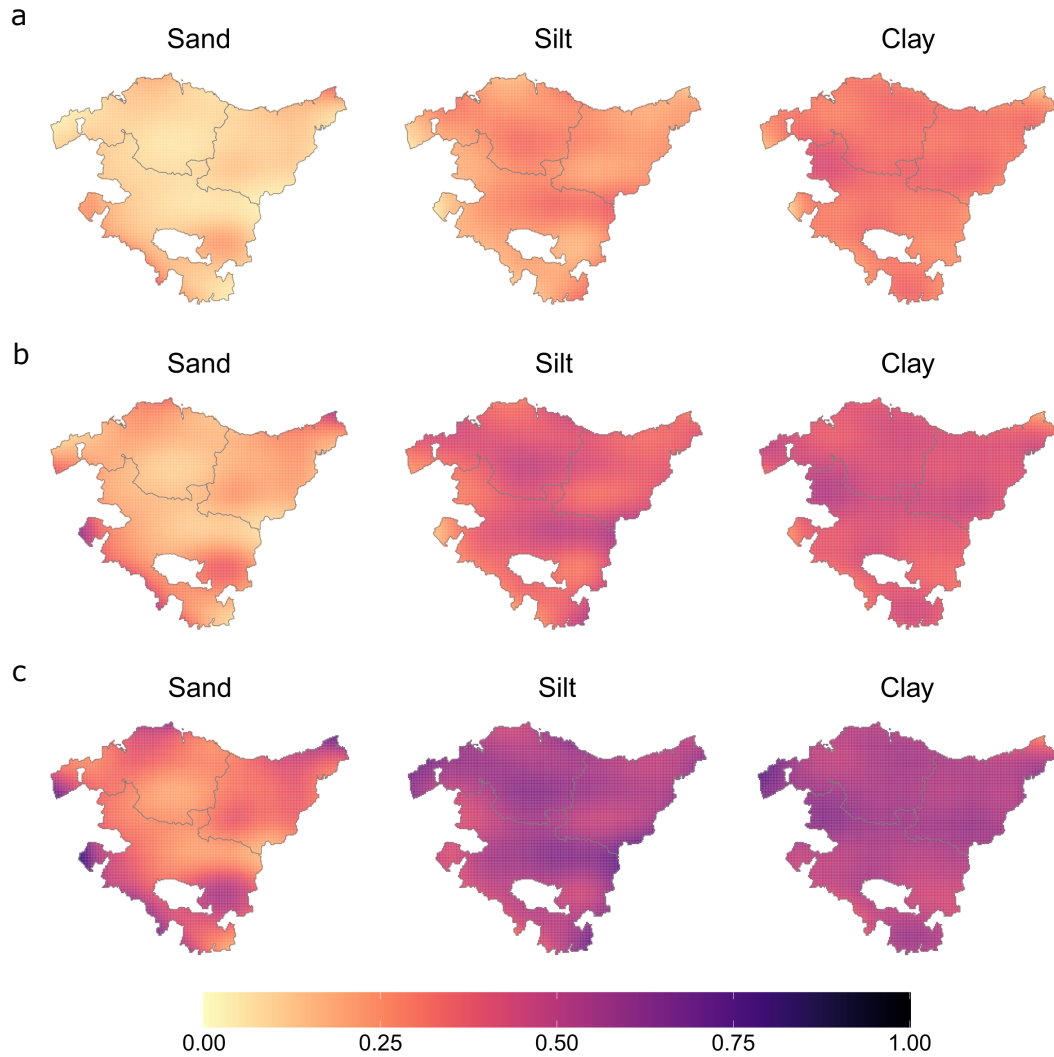


FIG 9. Posterior distribution of the smooth spatial term in the original space. Mean (row (b)) and 95% credible intervals (rows (a) and (c)) are depicted.

Finally, we produced predictions for the entire Basque Country, including the mean and standard deviation of the posterior predictive distributions, as well as the USDA textural classification derived from them (Figure 10). A key advantage of our modeling framework is the straightforward computation of predictive uncertainty. This stems from the isometric nature of the  $ilr$  transformation, which preserves distances and variances when mapping between the simplex and real space. Therefore, applying the inverse  $ilr$  transformation to posterior predictive samples in real space directly yields the full predictive distribution in the simplex.

This enables interpretation in terms of soil texture proportions and supports classification according to the USDA textural system, a widely adopted standard in soil science that categorizes soils by their relative contents of sand, silt, and clay (of Soil Survey, 1993). In this study, we computed the USDA textural class for each prediction point, generating a comprehensive soil texture classification map across the Basque Country (Figure 10).

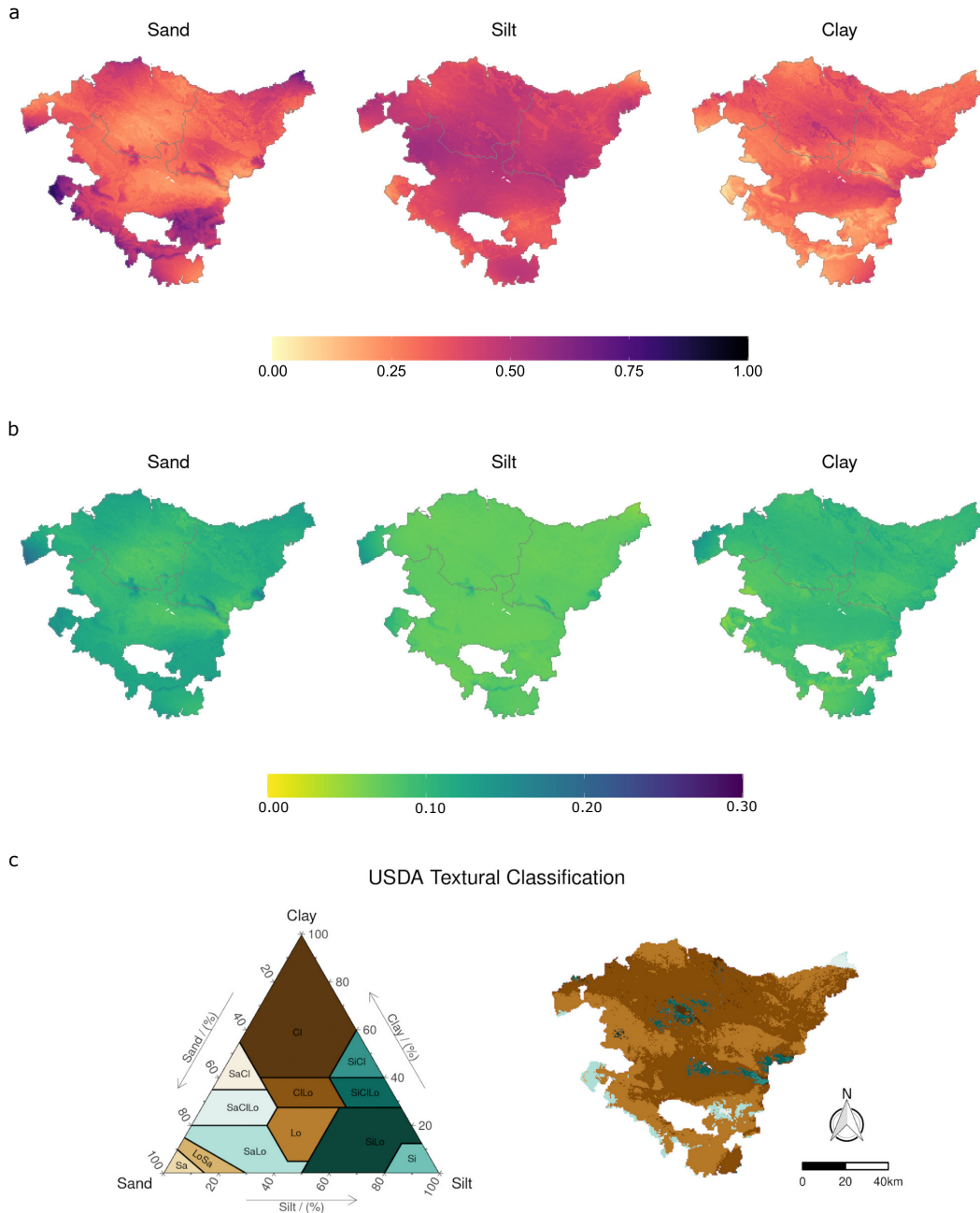


FIG 10. (a) Mean posterior predictive distribution for sand, silt and clay proportions. (b) Standard deviations of the posterior predictive distribution for sand, silt and clay proportions. (c) USDA textural classification in the simplex and in the Basque Country.

**9. Concluding remarks.** This work addressed key challenges in the modeling of spatial CoDa by proposing Bayesian GAM models for CoDa using penalized splines and tensor products within a flexible regression framework. Two main contributions were presented. First, we developed a Bayesian modeling framework that leverages the ilr transformation to incorporate smooth terms and spatial effects, preserving the geometry of the simplex. Sec-

ond, we introduced two novel Bayesian goodness-of-fit measures, BR-CoDa- $R^2$  and BM-CoDa- $R^2$ , which provide interpretable summaries of explained variability consistent with the Aitchison geometry. Simulation studies demonstrated the capacity of the proposed models to accurately recover underlying parameters and quantify explained variability. The real data application, predicting soil texture composition in the Basque Country, showcased the practical relevance of these models, highlighting the importance of spatial effects and covariates such as lithology, elevation, and slope. The `brms` package, together with our CoDa-specific extensions, facilitated the implementation and interpretation of results in the simplex space.

While the proposed Bayesian geoaddivitive modeling strategy can, in principle, employ alternative log-ratio transformations (e.g., `alr` or `clr`), the CoDa- $R^2$  measures presented here critically rely on the isometric property of the `ilr` transformation. Unlike `ilr`, both `alr` and `clr` are not isometries: they distort distances and angles relative to the Aitchison geometry, preventing a coherent decomposition of variability and rendering any derived  $R^2$  values difficult to interpret in terms of the original compositional structure. Therefore, the CoDa- $R^2$  measures proposed in this work are not directly transferable to models using `alr` or `clr` transformations.

The proposed BM-CoDa- $R^2$  relies on the assumption that the `ilr`-transformed coordinates of the response variable follow a multivariate normal distribution, as is standard in Gaussian Bayesian modeling. In contrast, the BR-CoDa- $R^2$  only requires posterior predictive samples of the `ilr` coordinates, and can therefore be used as a general-purpose validation metric in any Bayesian predictive framework that provides such samples. This includes flexible Bayesian machine learning methods, such as Bayesian additive regression trees (BART), Bayesian neural networks, or other simulation-based Bayesian approaches, provided that posterior predictive distributions in the real (`ilr`) space are available. Exploring these possibilities is a promising avenue for future research, especially in settings where classical parametric assumptions may not hold.

## APPENDIX A: CODE AVAILABILITY

All code used to implement the models described in this article is publicly available at the following GitHub repository: <https://github.com/jmartinez-minaya/CoDabrms/>

This repository includes:

- Scripts for simulating the datasets used in [section 7](#)
- Code for fitting the Bayesian CoDa-GAMs using the `brms` package
- Functions to compute BR-CoDa- $R^2$  and BM-CoDa- $R^2$

## APPENDIX B: ADDITIONAL FIGURES AND TABLES

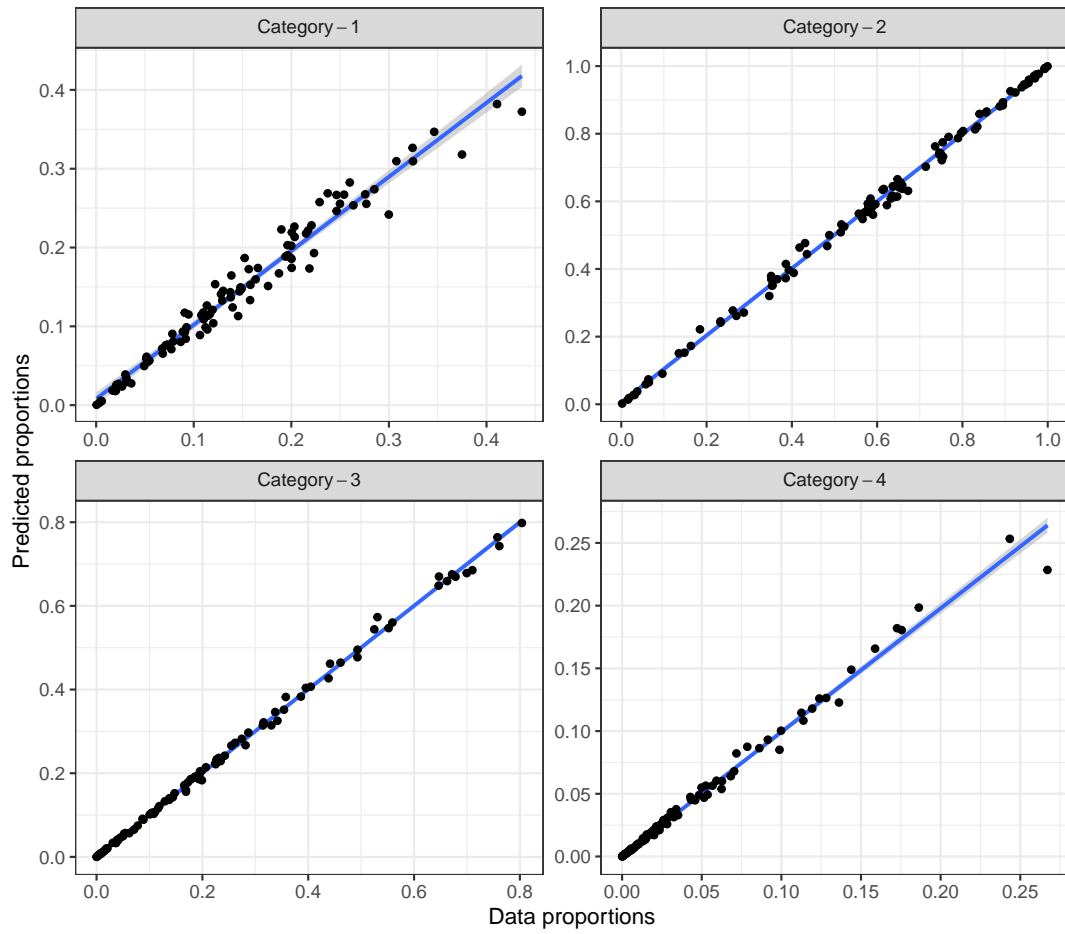


FIG 11. *Posterior predictive checks for the linear regression simulation example. Real values vs. mean of the posterior predictive distribution for each category in the composition. The blue line corresponds to a linear regression fit; proximity to the identity line indicating the model's ability to capture the linear structure.*

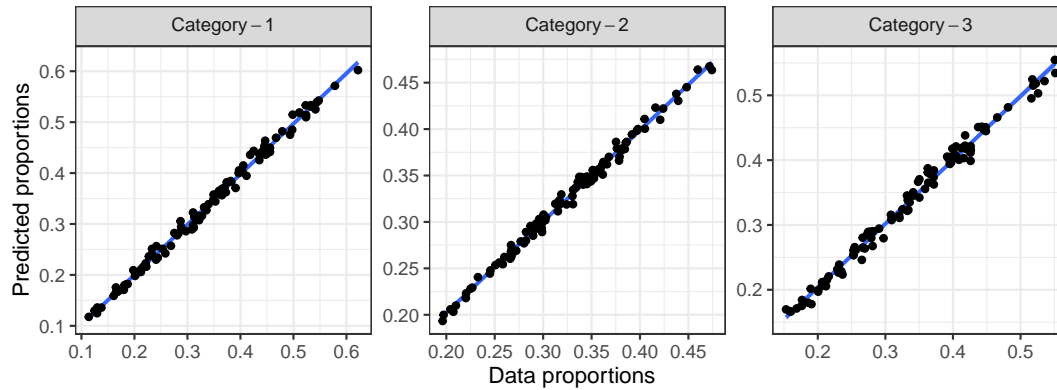


FIG 12. Posterior predictive checks for the GAM simulation example. Real values vs. mean of the posterior predictive distribution for each compositional category. The blue line represents the linear regression fit between observed and predicted values, illustrating the model's ability to capture the nonlinear structure.

**Funding.** Joaquín Martínez-Minaya, Lore Zumeta and Dae-Jin Lee gratefully acknowledge the Ministry of Science, Innovation and Universities (Spain) for research project PID2020-115882RB-I00.

## REFERENCES

- ADHIKARI, K., KHEIR, R. B., GREVE, M. B., BØCHER, P. K., MALONE, B. P., MINASNY, B., MCBRATNEY, A. B. and GREVE, M. H. (2013). High-resolution 3-D mapping of soil texture in Denmark. *Soil Science Society of America Journal* **77** 860–876.
- ADIN, A., KRAINSKI, E. T., LENZI, A., LIU, Z., MARTÍNEZ-MINAYA, J. and RUE, H. (2024). Automatic cross-validation in structured models: Is it time to leave out leave-one-out? *Spatial Statistics* **62** 100843. <https://doi.org/10.1016/j.spasta.2024.100843>
- AGUILAR, O. and BÜRKNER, P.-C. (2023). R2-D2 Shrinkage Priors: Prior Specification and Computational Strategies. *Electronic Journal of Statistics* **17** 2287–2321.
- AITCHISON, J. (1982). The statistical analysis of compositional data. *Journal of the Royal Statistical Society: Series B (Methodological)* **44** 139–160.
- AITCHISON, J. and LAUDER, I. J. (1985). Kernel Density Estimation for Compositional Data. *Applied Statistics* **34** 129. <https://doi.org/10.2307/2347365>
- AKPA, S. I., ODEH, I. O., BISHOP, T. F. and HARTEMINK, A. E. (2014). Digital mapping of soil particle-size fractions for Nigeria. *Soil Science Society of America Journal* **78** 1953–1966.
- AL-DHURAFI, N. A., MASSERAN, N. and ZAMZURI, Z. H. (2018). Compositional time series analysis for Air Pollution Index data. *Stochastic Environmental Research and Risk Assessment* **32** 2903–2911.
- AITCHISON, J. and SHEN, S. M. (1980). Logistic-normal distributions: Some properties and uses. *Biometrika* **67** 261–272.
- BALLABIO, C., PANAGOS, P. and MONATANARELLA, L. (2016). Mapping topsoil physical properties at European scale using the LUCAS database. *Geoderma* **261** 110–123. <https://doi.org/10.1016/j.geoderma.2015.07.006>
- BETANCOURT, M. and GIROLAMI, M. (2015). Hamiltonian Monte Carlo for Hierarchical Models. *Current Trends in Bayesian Methodology with Applications* 79–101. <https://doi.org/10.1201/b18502-5>
- BUCHANAN, S., TRIANTAFILIS, J., ODEH, I. O. A. and SUBANSINGHE, R. (2012). Digital soil mapping of compositional particle-size fractions using proximal and remotely sensed ancillary data. *Geophysics* **77**. <https://doi.org/10.1190/geo2012-0053.1>
- BÜRKNER, P.-C. (2017). brms: An R Package for Bayesian Multilevel Models Using Stan. *Journal of Statistical Software* **80** 1–28.
- CARPENTER, B., GELMAN, A., HOFFMAN, M. D., LEE, D., GOODRICH, B., BETANCOURT, M., BRUBAKER, M. A., GUO, J., LI, P. and RIDDELL, A. (2017). Stan: A probabilistic programming language. *Journal of Statistical Software* **76** 1–32. <https://doi.org/10.18637/jss.v076.i01>

- CHACÓN, J. E. and DUONG, T. (2010). Multivariate plug-in bandwidth selection with unconstrained pilot bandwidth matrices. *Test* **19** 375–398. <https://doi.org/10.1007/s11749-009-0168-4>
- CHAGAS, C. D. S., DE CARVALHO JUNIOR, W., BHERING, S. B. and CALDERANO FILHO, B. (2016). Spatial prediction of soil surface texture in a semiarid region using random forest and multiple linear regressions. *Catena* **139** 232–240.
- COMAS CUFÍ, M., THIÓ I FERNÁNDEZ DE HENESTROSA, S. et al. (2011). CoDaPack 2.0: a stand-alone, multi-platform compositional software.
- COMBETTES, P. L. and MÜLLER, C. L. (2020). Regression models for compositional data: General log-contrast formulations, proximal optimization, and microbiome data applications. *Statistics in Biosciences* 1–26.
- CREUS MARTÍ, I., MOYA, A. and SANTONJA, F.-J. (2022). Bayesian hierarchical compositional models for analysing longitudinal abundance data from microbiome studies. *Complexity* **2022** 4907527. <https://doi.org/10.1155/2022/4907527>
- DI MARZIO, M., PANZERA, A. and VENIERI, C. (2015). Non-parametric regression for compositional data. *Statistical Modelling* **15** 113–133. <https://doi.org/10.1177/1471082X14535522>
- EGOZCUE, J. J. and PAWLOWSKY-GLAHN, V. (2005). Groups of parts and their balances in compositional data analysis. *Mathematical Geology* **37** 795–828.
- EGOZCUE, J. J. and PAWLOWSKY-GLAHN, V. (2011). Basic concepts and procedures. *Compositional Data Analysis* 12–28.
- EGOZCUE, J. J., PAWLOWSKY-GLAHN, V., MATEU-FIGUERAS, G. and BARCELÓ-VIDAL, C. (2003). Isometric Logratio Transformations for Compositional Data Analysis. *Mathematical Geology* **35** 279–300. <https://doi.org/10.1023/A:1023818214614>
- EILERS, P. H. and MARX, B. D. (2021). *Practical smoothing: The joys of P-splines*. Cambridge University Press.
- FIGUEIRA, M., GUARNER, C., CONESA, D., LÓPEZ-QUÍLEZ, A. and KRISZTIN, T. (2025). Unveiling Land Use Dynamics: Insights from a Hierarchical Bayesian Spatio-Temporal Modelling of Compositional Data. *Journal of Agricultural, Biological and Environmental Statistics* **30** 283–308. <https://doi.org/10.1007/s13253-025-00678-6>
- GELMAN, A., HWANG, J. and VEHTARI, A. (2014). Understanding predictive information criteria for Bayesian models. *Statistics and computing* **24** 997–1016.
- GELMAN, A., GOODRICH, B., GABRY, J. and VEHTARI, A. (2019). R-squared for Bayesian Regression Models. *American Statistician* **73** 307–309. <https://doi.org/10.1080/00031305.2018.1549100>
- GOOLEY, L., HUANG, J., PAGE, D. and TRIANTAFILIS, J. (2014). Digital soil mapping of available water content using proximal and remotely sensed data. *Soil use and management* **30** 139–151.
- GU, C. and WAHBA, G. (1991). Minimizing GCV/GML Scores with Multiple Smoothing Parameters via the Newton Method. *SIAM Journal on Scientific and Statistical Computing* **12** 383–398. <https://doi.org/10.1137/0912021>
- HARTEMINK, A. E. and MCBRATNEY, A. (2008). A soil science renaissance. *Geoderma* **148** 123–129.
- HASTIE, T. and TIBSHIRANI, R. (1990). *Generalized Additive Models. Monographs on Statistics and Applied Probability*. Chapman and Hall, London.
- HENGL, T., DE JESUS, J. M., MACMILLAN, R. A., BATJES, N. H., HEUVELINK, G. B. M., RIBEIRO, E., SAMUEL-ROSA, A., KEMPEN, B., LEENAARS, J. G. B., WALSH, M. G. and GONZALEZ, M. R. (2014). SoilGrids1km - Global soil information based on automated mapping. *PLoS ONE* **9**. <https://doi.org/10.1371/journal.pone.0105992>
- HIJAZI, R. H. (2008). Residuals Analysis of the Dirichlet Regression. **September**.
- HIJAZI, R. H. and JERNIGAN, R. W. (2009). Modeling Compositional Data Using Dirichlet Regression Models. *Journal of Applied Probability and Statistics* **4** 2009.
- LEININGER, T. J., GELFAND, A. E., ALLEN, J. M. and SILANDER, J. A. (2013). Spatial Regression Modeling for Compositional Data With Many Zeros. *Journal of Agricultural, Biological, and Environmental Statistics* **18** 314–334. <https://doi.org/10.1007/s13253-013-0145-y>
- LIN, W., SHI, P., FENG, R. and LI, H. (2014). Variable selection in regression with compositional covariates. *Biometrika* **101** 785–797.
- MARTINEZ, E. Z., ACHCAR, J. A., ARAGON, D. C. and BRUNHEROTTI, M. A. A. (2020). A Bayesian analysis for pseudo-compositional data with spatial structure. *Statistical Methods in Medical Research* **29** 1386–1402. <https://doi.org/10.1177/0962280219862587>
- MARTÍNEZ-MINAYA, J. and RUE, H. (2024). A flexible Bayesian tool for CoDa mixed models: logistic-normal distribution with Dirichlet covariance. *Statistics and Computing* **34** 116.
- MOTA-BERTRAN, A., SAEZ, M. and COENDERS, G. (2022). Compositional and Bayesian inference analysis of the concentrations of air pollutants in Catalonia, Spain. *Environmental Research* **204** 112388. <https://doi.org/10.1016/j.envres.2021.112388>

- NIANG, M. A., NOLIN, M. C., JÉGO, G. and PERRON, I. (2014). {Digital Mapping of Soil Texture Using RADARSAT-2 Polarimetric Synthetic Aperture Radar Data}. *Soil Science Society of America Journal* **78** 673–684.
- NUSSBAUM, M., WALTHERT, L., FRAEFEL, M., GREINER, L. and PAPRITZ, A. (2017). Mapping of soil properties at high resolution in Switzerland using boosted geosadditive models. *SOIL* **3** 191–210. <https://doi.org/10.5194/soil-3-191-2017>
- OF SOIL SURVEY, U. S. D. (1993). *Soil survey manual* **18**. US Department of Agriculture.
- PAWLOWSKY-GLAHN, V. and BUCCIANTI, A. (2011). *Compositional data analysis: Theory and applications*. John Wiley & Sons.
- PAWLOWSKY-GLAHN, V. and EGOZCUE, J. J. (2001). Geometric approach to statistical analysis on the simplex. *Stochastic Environmental Research and Risk Assessment* **15** 384–398.
- PAWLOWSKY-GLAHN, V., EGOZCUE, J. J. and TOLOSANA-DELGADO, R. (2015). *Modeling and analysis of compositional data*. John Wiley & Sons.
- PAWLOWSKY-GLAHN, V. and EGOZCUE, J. J. (2016). Spatial analysis of compositional data: a historical review. *Journal of Geochemical Exploration* **164** 28–32.
- PIRZAMANBEIN, B., LINDSTRÖM, J., POSKA, A. and GAILLARD, M.-J. (2018). Modelling spatial compositional data: Reconstructions of past land cover and uncertainties. *Spatial statistics* **24** 14–31.
- POGGIO, L. and GIMONA, A. (2017). 3D mapping of soil texture in Scotland. *Geoderma Regional* **9** 5–16.
- SUSIN, A., WANG, Y., LÊ CAO, K.-A. and CALLE, M. L. (2020). Variable selection in microbiome compositional data analysis. *NAR Genomics and Bioinformatics* **2** lqaa029.
- SWETHA, R., BENDE, P., SINGH, K., GORTHI, S., BISWAS, A., LI, B., WEINDORF, D. C. and CHAKRABORTY, S. (2020). Predicting soil texture from smartphone-captured digital images and an application. *Geoderma* **376** 114562.
- THOMAS, S. (2020). bayesGAM: Fit Multivariate Response Generalized Additive Models using Hamiltonian Monte Carlo R package version 0.0.1.
- VAN DEN BOOGAART, K. G., TOLOSANA-DELGADO, R. and BREN, M. (2021). compositions: Compositional Data Analysis R package version 2.0-1.
- VEHTARI, A., GELMAN, A. and GABRY, J. (2017). Practical Bayesian model evaluation using leave-one-out cross-validation and WAIC. *Statistics and Computing* **27** 1413–1432. <https://doi.org/10.1007/s11222-016-9696-4>
- VEHTARI, A., GELMAN, A., GOODRICH, B. and GABRY, J. (2025). Bayesian  $R^2$  online resource. [https://avehtari.github.io/bayes\\_R2/bayes\\_R2.html](https://avehtari.github.io/bayes_R2/bayes_R2.html). Accessed: June 2025.
- WADOUX, A. M. J. C. and MOLNAR, C. (2021). Beyond prediction: methods for interpreting complex models of soil variation.
- WANG, Z., WANG, H. and WANG, S. (2019). Linear mixed-effects model for multivariate longitudinal compositional data. *Neurocomputing* **335** 48–58. <https://doi.org/10.1016/j.neucom.2019.01.043>
- WEN ZHANG, S., YANG SHEN, C., YANG CHEN, X., CHUN YE, H., FANG HUANG, Y. and LAI, S. (2013). Spatial Interpolation of Soil Texture Using Compositional Kriging and Regression Kriging with Consideration of the Characteristics of Compositional Data and Environment Variables. *Journal of Integrative Agriculture* **12** 1673–1683. [https://doi.org/10.1016/S2095-3119\(13\)60395-0](https://doi.org/10.1016/S2095-3119(13)60395-0)
- WOOD, S. N. (2017). *Generalized additive models: an introduction with R*. CRC press.
- ZHANG, X., BONDELL, H. D. and REICH, B. J. (2020). Bayesian predictive priors in high-dimensional regression models. *Journal of the American Statistical Association* **115** 1123–1133.
- ZHOU, S., ZHOU, K., WANG, J., YANG, G. and WANG, S. (2018). Application of cluster analysis to geochemical compositional data for identifying ore-related geochemical anomalies. *Frontiers of Earth Science* **12** 491–505.